Two-tone frequency-modulation spectroscopy for quantitative measurements of gaseous species: Theoretical, numerical, and experimental investigation of line shapes

Avetisov, V. G; Kauranen, P

Published in:
Applied Optics

DOI:
10.1364/AO.35.004705

1996

Two-tone frequency-modulation spectroscopy for quantitative measurements of gaseous species: theoretical, numerical, and experimental investigation of line shapes

V. G. Avetisov and P. Kauranen

The capability of retrieving spectral information from line shapes recorded by two-tone frequency-modulation spectroscopy (TTFMS) is investigated. A TTFMS theory accounting for dispersion and nonlinear distortion of diode laser frequency modulation response is presented. The adequacy of the theory for a detailed modeling of line shapes recorded with high resolution is examined. An extensive error analysis of line parameters (i.e., width, intensity, and line center) retrieved by a nonlinear least-squares fitting procedure is made. Plots of residual errors with characteristic signatures that are due to incorrectly assigned modulation parameters and choice of line profile are presented. In least-squares fits to experimental oxygen data with a Voigt profile influence from collisional (Dicke) narrowing is clearly exhibited, and when we used a collisionally narrowed line profile deviations of the model were reduced to less than 0.2%. We demonstrate that accurate quantitative measurements by TTFMS over a wide range of concentrations, temperatures, and pressures are possible.

Key words: Frequency-modulation spectroscopy, high-resolution spectroscopy, absorption spectroscopy.

1. Introduction

Two-tone frequency-modulation spectroscopy (TTFMS) has gained large interest in gas species measurements for which high sensitivity is required.[1–8] Applying TTFMS for quantitative measurements over a wide range of concentrations, temperatures, or pressures requires information about the line parameters and an adequate theory of the heterodyne detected signal. The line parameter data can be found with varying accuracy in the literature and in databases.[9] However, in the near IR, where cheap and reliable diode lasers can be employed, tabulated data are insufficient and it is likely that the line parameters of the transition of interest must be measured separately. A TTFMS theory in turn has been derived,[10–12] however in high-resolution measurements of line parameters or quantitative measurements of gas species the available theory might have limited validity. In this study we examine the TTFMS theory and investigate the capability of TTFMS for quantitative measurements by analyzing the accuracy with which line parameters can be retrieved by a least-squares fitting procedure. In this connection the high sensitivity of TTFMS may also be useful exclusively for line parameter measurements in situations for which sufficient sensitivity is not achievable for direct detection.

High-resolution measurements of multiple line parameters in molecular band structures are routinely performed by least-squares fits to directly detected spectra.[13–15] Also, quantitative measurements of gas species by least-squares fits to observed data have become common practice.[16–19] When the instrumental distortion or noise level is of the order of a few percent of the signal amplitude, the computationally simple Voigt profile adequately describes a recorded line shape. Today experimental methods allow recording of line shapes with instrumental distortions almost as small as 10^{-3}, and collisional (Dicke) narrowing[20] of spectral lines is readily observable.[21–24] If collisional narrowing is significant, a

When this research was done both authors were with the Division of Atomic Physics, Lund Institute of Technology, P.O. Box 118, S-221 00 Lund, Sweden. V. G. Avetisov is now with Norsk Elektro Optikk A/S, Solheimveien 62A, P.O. Box 384, 1471 Skarer, Norway.

Received 13 October 1995; revised manuscript received 21 March 1996.

0003-6935/96/244705-19$10.00/0

more elaborate line profile provides a better fit to data and extracts line parameters with higher accuracy.

The requirement for high sensitivity in gas species detection brought about the development of spectroscopic methods that make use of modulation schemes, among which the most widely adopted employ frequency modulation (FM). Depending on the number of applied modulation tones, the choice of modulation frequency relative to the widths of the studied absorption features, and the detection frequency, the FM techniques are commonly referred to as wavelength modulation spectroscopy (WMS),[25] frequency-modulation spectroscopy (FMS),[26] and TTFMS.[27,28] The fundamental feature is phase-sensitive heterodyne detection of an absorption induced beat in the laser intensity at a frequency related to the applied modulation frequency(ies). By this movement of the detection band to higher frequencies one can reduce the influence from low-frequency ($1/f$) noise. The FM techniques are frequently used with diode lasers, which one can easily modulate by superimposing a sine-wave signal directly onto the drive current. WMS normally uses modulation frequencies of a few hundred kilohertz and a large modulation index, whereas FMS and TTFMS employ a moderate modulation index and modulation frequencies that are comparable with or larger than the width of the absorbing feature. The ultimate sensitivity achievable with the different FM schemes has been investigated in several studies.[11,29–32] Although shot-noise-limited detection at 10^{-7}–10^{-8} fractional absorption is possible with FMS[33,34] and TTFMS,[35,36] in practice the sensitivity is limited to approximately 10^{-6} by optical interference effects. Nevertheless, this detection limit should allow line shapes from absorptions as small as 10^{-3} to be modeled with systematic discrepancies at a level limited by the instrumental distortion only.

The theoretical approach commonly adopted for WMS is limited to low modulation frequencies, whereas the theoretical approach for FMS and TTFMS that we use in this study is valid for arbitrary modulation frequencies.[37] By WMS with second-harmonic ($2f$) detection the line parameters can be measured from the dependence of the signal amplitude with the modulation amplitude.[38–40] With this method the line shape can be measured at the line center frequency only, which makes it difficult to evaluate the adequacy of the applied theory and line profile, and hence the accuracy of the retrieved line parameters. Quantitative measurements of gasdynamic parameters by WMS have been demonstrated[41] by using a linear least-squares fitting procedure with which literature values of the line parameters were adopted. High-resolution measurement of line parameters by FMS has been demonstrated by nonlinear least-squares fitting weak absorptions.[42] Also a high-resolution measurement of line parameters with TTFMS has been demonstrated.[43] In Ref. 43 a recorded air-broadened oxygen line shape was least-squares fitted with systematic discrepancies below 1% by using a Voigt profile, however adjusting the modulation and the line parameters simultaneously in the fit exposed strong correlations. In particular, the FM index parameter correlated with the broadening and line intensity parameters.

Although quantitative measurements of a gas species in a highly varying environment require that line-shape changes be considered, only a few implementations with FM techniques have been presented in which measured data are modeled. Accurate modeling requires an adequate theory of the modulated laser light and its interaction with the gas species, which also includes the choice of an appropriate line profile. In a nonlinear least-squares fit of the heterodyne detected line shape some of the modulation parameters correlate with the line profile parameters, i.e., an error in the assignment of the modulation parameters propagates into the retrieval of the line parameters. As a result the set of parameters that provides the best fit to data is not unique. Owing to the correlations between the increased number of variables the retrieval accuracy of the FM techniques is expected to vary with the modulation condition and to be somewhat lower than with direct detection. Yet, a comparative study of the ultimate retrieval accuracy obtainable with the different FM techniques in high-resolution measurements has to be done.

The aim of this study is to extend the applicability of TTFMS in the direction of performing reliable quantitative measurements. In Section 2 we introduce a TTFMS theory that extends the research of Cooper and Warren.[11,12] In our representation we derive expressions that account for dispersion, and we specify ranges of the modulation parameters for which different complexity levels of the theory can be applied. Also nonlinear distortion of the diode laser modulation response is introduced in the theory and evaluated. In Section 3 we describe the nonlinear least-squares fitting procedure and the different line profile functions that were used to model the TTFMS line shapes. In Section 4 we analyze numerically the correlations among the modulation and line profile parameters in a least-squares fit over a wide range of parameter values. To provide support for evaluating the results from a modeling of experimental data we present different plots of residuals (observed minus calculated) with characteristic signatures induced by incorrectly assigned modulation parameters. Investigation of the FM index-induced errors is supplemented by a statistical approach, with which retrieval uncertainties from synthetic spectra with random noise can be estimated. In Section 5 we evaluate the effect of dispersion numerically and demonstrate it experimentally. In Section 6 we demonstrate numerically the systematic difference in TTFMS between collisionally (Dicke) narrowed line shapes and the Voigt profile by the residual obtained from a least-squares fit. In Section 7 we test the analysis experimentally by least-squares fits to oxygen data.

An extensive experimental investigation of high-

resolution measurements of line parameters by TTFMS together with a comparison to direct detection will be presented in a separate paper,[44] in which we also discuss the essential experimental considerations for achieving high modeling accuracy.

2. Two-Tone Frequency-Modulation Spectroscopy Theory

A. General Approach

A diode laser can be two-tone frequency modulated by imposing two closely spaced radio frequency signals $\nu_1 \equiv \nu_m + \frac{1}{2}\Omega$ and $\nu_2 \equiv \nu_m - \frac{1}{2}\Omega$ directly to the diode laser drive current. The amplitude- and phase-modulated electric field produced can be written as

$$E_1(t) = E_0[1 + M\sin(2\pi\nu_1 t + \Psi)][1 + M\sin(2\pi\nu_2 t + \Psi)] \times \exp\{i2\pi\nu_c t + i\beta[\sin(2\pi\nu_1 t) + \sin(2\pi\nu_2 t)]\}, \quad (1)$$

where E_0 is the amplitude of the laser field, ν_c is the laser carrier frequency, β is the FM index, M is the amplitude modulation (AM) index, and Ψ is the phase difference between AM and FM. Generally, the generator frequencies ν_m and $\frac{1}{2}\Omega$ are chosen such that ν_m is comparable with or larger than the absorption halfwidth to obtain optimum sensitivity, and the intermediate frequency $\Omega = \nu_1 - \nu_2$ that is detected is small in comparison with the modulation frequencies but large enough to avoid low-frequency $(1/f)$ noise, i.e., typically 5–20 MHz for diode lasers. Since the modulation frequencies are closely spaced, it is assumed that they both induce the same β, M, and Ψ in the electric field.

Expanding the phase modulation components in Eq. (1) in terms of Bessel functions $J_n(\beta)$ and the AM components into complex exponentials yields

$$E_1(t) = E_0\exp(i2\pi\nu_c t)\sum_{n,m=-\infty}^{+\infty} r_n r_m \exp[i2\pi(n\nu_1 + m\nu_2)t], \quad (2)$$

where

$$r_n(\beta, M, \Psi) \equiv J_n(\beta) + \frac{M}{2i}[J_{n-1}(\beta)\exp(i\Psi) - J_{n+1}(\beta)\exp(-i\Psi)]. \quad (3)$$

Figure 1 shows schematically the spectral distribution of the two-tone frequency-modulated laser field for $\beta = 1.0$, $M = 0$, and with the intermediate frequency Ω greatly exaggerated for illustration. The central component ($n = m = 0$) is the laser carrier and the sidebands are at frequencies $\nu_c + n\nu_1 + m\nu_2$, where $n, m = 0, \pm1, \pm2, \ldots$. The sidebands appear in groups symmetrically (in pairs) around the laser carrier frequency, which we refer to as sideband groups. Note that a sideband group contains intermodulation products of different orders, e.g., the first-order sideband group contains a third-order intermodulation product $(2\nu_1 - \nu_2)$.

An electric field interacts with a sample according

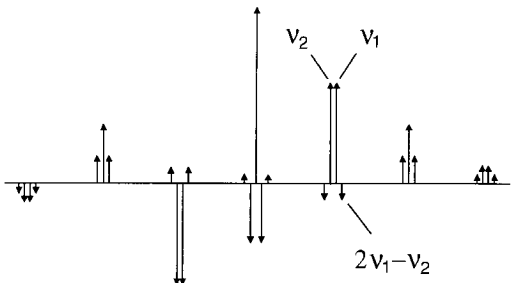

Fig. 1. Spectral distribution of the laser field, two-tone frequency modulated at ν_1 and ν_2, with $\beta = 1.0$ and $M = 0$.

to

$$E(t) = E_0\exp[i2\pi\nu t - \tfrac{1}{2}\alpha(\nu) - i\phi(\nu)], \quad (4)$$

where $\alpha(\nu)$ is the dimensionless intensity absorbance at frequency ν, and $\phi(\nu)$ is the optical phase shift. Passing the frequency-modulated beam through a sample, each frequency component $\nu_c + n\nu_1 + m\nu_2$ (Fig. 1) experiences different attenuations and phase shifts. Thus, the electric field after interaction with the sample is

$$E_2(t) = E_0\exp(i2\pi\nu_c t)\sum_{n,m=-\infty}^{+\infty} r_n r_m \exp[i2\pi(n\nu_1 + m\nu_2)t]\exp(-\tfrac{1}{2}\alpha_{n,m} - i\phi_{n,m}), \quad (5)$$

where $\alpha_{n,m} \equiv \alpha(\nu_c + n\nu_1 + m\nu_2)$ and $\phi_{n,m} \equiv \phi(\nu_c + n\nu_1 + m\nu_2)$. The intensity detected by a photodetector is $I(t) = c\varepsilon_0 EE^*/2$ or

$$I(t) = \frac{c\varepsilon_0}{2}E_0^{\,2}\sum_{\substack{n,m,\\ n',m'}} r_n r_m r_{n'}^* r_{m'}^* \exp\{i2\pi[(n-n')\nu_1 + (m-m')\nu_2]t\} \times \exp[-\tfrac{1}{2}(\alpha_{n,m} + \alpha_{n',m'}) - i(\phi_{n,m} - \phi_{n',m'})]. \quad (6)$$

The time-varying intensity components, arising from the heterodyning of adjacent frequency sidebands at $\pm\Omega$, are obtained for $n - n' = \pm1$ and $m - m' = \mp1$. Summing the beat signals at Ω of Eq. (6) produces

$$I_\Omega(t) = \frac{c\varepsilon_0}{2}E_0^{\,2}\exp(-2\pi i\Omega t)\sum_{n,m} r_n r_m r_{n+1}^* r_{m-1}^* \times \exp[-\tfrac{1}{2}(\alpha_{n,m} + \alpha_{n+1,m-1}) - i(\phi_{n,m} - \phi_{n+1,m-1})] + \text{c.c.} \quad (7)$$

The simplifying assumption generally made in the representation of TTFMS that the intermediate frequency Ω is small in relation to the spectral variations in α and ϕ, i.e., sidebands spaced at Ω experience the same absorption and dispersion, yields the approximation $\nu_1 \approx \nu_2 \approx \nu_m$.[10–12,27,28,30] When we apply this approximation in Eq. (7) the dispersion components vanish. In our analysis we retain the dispersion in order to obtain a more general signal representation that can be used to evalu-

ate the effect of dispersion for various experimental configurations. We anticipate that the absorbances measured by TTFMS are not more than a few percent and that Ω in some sense is still small in comparison with the spectral variations in ϕ, which implies that $|\phi_{n,m} - \phi_{n+1,m-1}| \ll 1$. Thus the approximation

$$\begin{aligned}&\exp[-\tfrac{1}{2}(\alpha_{n,m} + \alpha_{n+1,m-1}) - i(\phi_{n,m} - \phi_{n+1,m-1})]\\ &= \exp[-\tfrac{1}{2}(\alpha_{n,m} + \alpha_{n+1,m-1})][1 - i(\phi_{n,m} - \phi_{n+1,m-1})\\ &\quad - \tfrac{1}{2}(\phi_{n,m} - \phi_{n+1,m-1})^2 + \ldots]\\ &\cong \exp[-\tfrac{1}{2}(\alpha_{n,m} + \alpha_{n+1,m-1})] - i(\phi_{n,m} - \phi_{n+1,m-1}) \quad (8)\end{aligned}$$

can be applied in Eq. (7), which separates the absorption and dispersion components, yielding

$$I_\Omega(t) = (I_\Omega{}^\alpha + \Im_\Omega{}^\phi)\cos(2\pi\Omega t) + (I_\Omega{}^\phi + \Im_\Omega{}^\alpha)\sin(2\pi\Omega t), \quad (9)$$

where

$$I_\Omega{}^\alpha \equiv c\varepsilon_0 E_0{}^2 \sum_{n,m} \mathrm{Re}(r_n r_m r^*_{n+1} r^*_{m-1}) \times \exp[-\tfrac{1}{2}(\alpha_{n,m} + \alpha_{n+1,m-1})], \quad (10a)$$

$$I_\Omega{}^\phi \equiv c\varepsilon_0 E_0{}^2 \sum_{n,m} \mathrm{Re}(r_n r_m r^*_{n+1} r^*_{m-1})(\phi_{n+1,m-1} - \phi_{n,m}), \quad (10b)$$

$$\Im_\Omega{}^\alpha \equiv c\varepsilon_0 E_0{}^2 \sum_{n,m} \mathrm{Im}(r_n r_m r^*_{n+1} r^*_{m-1}) \times \exp[-\tfrac{1}{2}(\alpha_{n,m} + \alpha_{n+1,m-1})], \quad (10c)$$

$$\Im_\Omega{}^\phi \equiv c\varepsilon_0 E_0{}^2 \sum_{n,m} \mathrm{Im}(r_n r_m r^*_{n+1} r^*_{m-1})(\phi_{n,m} - \phi_{n+1,m-1}). \quad (10d)$$

The correctness of the approximation in Eq. (8) can be determined mainly by the second-order term in the Taylor expansion. By using a Voigt profile to calculate different line shapes we verified numerically that

$$|\phi_{n,m} - \phi_{n+1,m-1}| \le |\phi_{0,0} - \phi_{1,-1}| \cong \tfrac{1}{2}\,\alpha(\nu_0)\,\frac{\Omega}{\Delta} \left(\frac{\Omega}{\Delta} < 0.2\right),$$

where $\alpha(\nu_0)$ is the absorbance at the line center position ν_0, and Δ is the halfwidth at half-maximum (HWHM) of the absorbing feature. Then, for the approximation in Eq. (8) [and thus Eq. (9)] to be valid with a 10^{-3} relative error the following requirement can be specified:

$$\alpha(\nu_0)\,\frac{\Omega}{\Delta} < 4 \times 10^{-3}, \quad (11)$$

which is generally fulfilled for the absorbances that are measured with TTFMS.

The light intensity described by Eq. (9) consists of two time-varying components, both of which are proportional to absorption and dispersion. The most important part is the quadrature component $\sim\cos(2\pi\Omega t)$, which is proportional to the absorption through $I_\Omega{}^\alpha$. In general, in the phase-sensitive detection of the time-varying intensity the detection phase can be adjusted to give an optimum signal amplitude. However, as we show in the following, this involves a part of the dispersion component $I_\Omega{}^\phi$ that falls within the detection angle. The absorption $\Im_\Omega{}^\alpha$ and dispersion $\Im_\Omega{}^\phi$ components that originate from the imaginary part of $r_n r_m r^*_{n+1} r^*_{m-1}$ are negligible in most situations and vanish for $\Psi = \pm\pi/2$ or $M = 0$.

The spectral line shapes of the absorption $I_\Omega{}^\alpha$ and dispersion $I_\Omega{}^\phi$ components are symmetrical with respect to the line center, whereas the absorption $\Im_\Omega{}^\alpha$ and dispersion $\Im_\Omega{}^\phi$ are asymmetrical. By calculating various line shapes using Eqs. (10a)–(10d), we estimated the relative peak-to-peak (pp) values of $I_\Omega{}^\alpha$, $I_\Omega{}^\phi$, $\Im_\Omega{}^\alpha$, and $\Im_\Omega{}^\phi$ in the ranges of $0.3 \le \beta \le 1.3$, $\nu_m/\Delta \ge 0.3$, and $\Omega/\Delta < 0.1$. By regression analysis of the obtained data the following approximate expressions were attained:

$$(I_\Omega{}^\phi)_{\mathrm{pp}}/(I_\Omega{}^\alpha)_{\mathrm{pp}} \approx A\,\frac{\Omega}{\Delta}, \quad 0.5 \le A < 1.5, \quad (12a)$$

$$(\Im_\Omega{}^\phi)_{\mathrm{pp}}/(I_\Omega{}^\alpha)_{\mathrm{pp}} \approx \sqrt{\beta}\left(\frac{\Omega}{\Delta}\right)^2\left[1 + \left(\frac{\Delta}{\nu_m}\right)^2\right]\frac{M}{\beta}\,|\cos\Psi|, \quad (12b)$$

$$(\Im_\Omega{}^\alpha)_{\mathrm{pp}}/(\Im_\Omega{}^\phi)_{\mathrm{pp}} \approx 10. \quad (12c)$$

The value of A in approximation (12a) varies with the ratio ν_m/Δ as is shown in Section 5, in which it is investigated in detail. The magnitude of the dispersion component $I_\Omega{}^\phi$ can amount to several percent of the absorption component $I_\Omega{}^\alpha$, e.g., if low pressure Doppler-limited line shapes are measured, however, since it appears in quadrature with $I_\Omega{}^\alpha$ [Eq. (9)], its influence is reduced after phase-sensitive detection that has been optimized for maximum signal amplitude. However, a reduction significantly below 1% of the heterodyne-detected signal might be difficult to accomplish. For example, if Ω = 20 MHz and Δ = 500 MHz, i.e., a typical Doppler halfwidth in the near IR, approximation (12a) with $A = 1$ is approximately 0.04. In this case, the optimum signal amplitude is found at 2.5° phase shift relative to the quadrature component $\sim\cos(2\pi\Omega t)$, and a phase-sensitive detected signal contains at least 0.2% contribution from the dispersion. Furthermore, if the optimum amplitude is found with 1% accuracy, the corresponding phase adjustment is ±8°, which may result in 0.7% dispersion contribution after phase-sensitive detection. Accordingly, in accurate modeling of TTFMS line shapes dispersion cannot be completely disregarded. The dispersion should be either considered in the employed theory or estimated for the experimental situation in order to specify the required phase adjustment. On the other hand if $\Omega/\Delta <$ 0.005 the dispersion contribution that originates from a phase adjustment uncertainty of ±8° is smaller than 10^{-3}, which is negligible.

The range of the ratio Ω/Δ in which the quadrature dispersion component $\Im_\Omega{}^\phi$ is smaller than 10^{-3} of the absorption component $I_\Omega{}^\alpha$ and is thus negligible can be estimated by approximation (12b). For an AM–FM index ratio of $M/\beta = 0.1$, which is quite large for diode lasers, and with unfavorably chosen values such as $\nu_m/\Delta = 0.3$, $\beta = 1.3$, and $\Psi = \pi$, we attain the requirement that $\Omega/\Delta < 0.03$. Thus, when we measure a line shape with a halfwidth of $\Delta = 500$ MHz, the intermediate frequency should be constrained to $\Omega < 15$ MHz. For diode lasers, as is discussed in Subsection 4.C, Ψ is close to $\pi/2$, and hence the quadrature dispersion component $\Im_\Omega{}^\phi$ is smaller, abating the requirement for the ratio Ω/Δ.

Although the in-phase absorption component $\Im_\Omega{}^\alpha$ is an order of magnitude larger than $\Im_\Omega{}^\phi$, its influence is reduced to a negligible level when the detection phase is adjusted for the quadrature component. For the same parameter values that were used to estimate $\Im_\Omega{}^\phi$ above, a detection phase adjustment of $\pm 6°$ assures that $\Im_\Omega{}^\alpha$ is smaller than 10^{-3}.

As a result of the above analysis we can neglect the absorption $\Im_\Omega{}^\alpha$ and dispersion $\Im_\Omega{}^\phi$ components if $\Omega/\Delta < 0.03$, which is easy to satisfy experimentally. Then phase-sensitive detection of the time-varying intensity described by Eq. (9) produces

$$I_\Omega(\theta) \cong I_\Omega{}^\alpha \cos\theta + I_\Omega{}^\phi \sin\theta, \tag{13}$$

where θ is the detection phase, i.e., the phase difference between the photodetected quadrature component and the local oscillator reference.

It is interesting to know to what extent the approximation $\nu_1 \approx \nu_2 \approx \nu_m$ is valid when it is applied in calculations of the absorption component $I_\Omega{}^\alpha$ by Eq. (10a), which is then simplified to

$$I_\Omega{}^\alpha \cong c\varepsilon_0 E_0{}^2 \sum_{n,m} \mathrm{Re}(r_n r_m r_{n+1}^* r_{m-1}^*) \times \exp\{-\alpha[\nu_c + (n+m)\nu_m]\}. \tag{14}$$

This is the expression generally used in the literature to calculate TTFMS line shapes. By comparing line shapes generated by Eq. (10a) and relation (14), respectively, for various linewidths and modulation parameters we found that they differ by less than 10^{-3} if

$$\frac{\Omega}{\Delta} < \frac{0.02}{1 + (\Delta/\nu_m)^2}. \tag{15}$$

Thus, if the intermediate frequency Ω is chosen such that it satisfies inequality (15) for the recorded line shape, the more simple relation (14) can be used in the modeling of the line shape. With a halfwidth of $\Delta = 500$ MHz and $\nu_m/\Delta = 1$, inequality (15) can be fulfilled when $\Omega < 5$ MHz.

An illustrative way of writing relation (14) is feasible by setting $k = n + m$:

$$I_\Omega{}^\alpha = c\varepsilon_0 E_0{}^2 \sum_k R_k \exp[-\alpha(\nu_c + k\nu_m)], \tag{16}$$

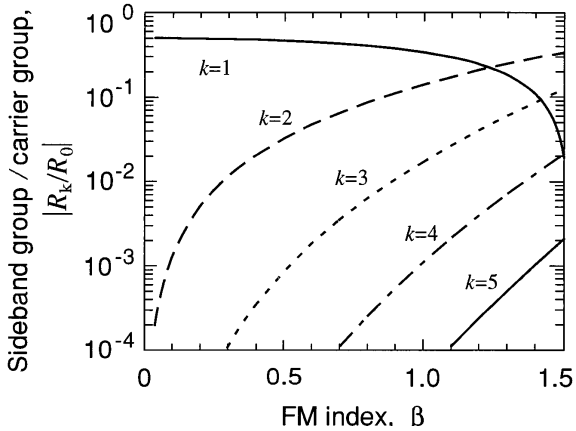

Fig. 2. Ratio of the first five sideband group amplitudes to the carrier group amplitude versus the FM index β with $M = 0$.

where

$$R_k(\beta, M, \Psi) \equiv \sum_n \mathrm{Re}(r_n r_{k-n} r_{n+1}^* r_{k-n-1}^*) \tag{17}$$

is the amplitude of the kth sideband group. The number of sideband groups to be accounted for in calculating line shapes depends on the FM index and the required modeling accuracy. The order of the highest sideband group can be estimated from Fig. 2, where the ratio of the first five sideband group amplitudes to the carrier group (i.e., $|R_k|/|R_0|$) is plotted as a function of the FM index β. For example, for $\beta = 1.0$ we have $|R_3|/|R_0| \approx 0.02$ and $|R_4|/|R_0| \approx 10^{-3}$, which implies that (for $\beta \leq 1$) sideband groups with higher than third order can be neglected.

Finally, it should be mentioned that the laser linewidth, which is not considered in our analysis, can be included by means of a convolution.

B. Second-Order Nonlinear Distortion

Nonlinear distortion of a diode laser modulation response may be caused by different factors such as leakage current,[45] gain suppression and spatial hole burning,[46] and the magnitude of the distortion varies with modulation frequency and FM index.[47] In a detailed modeling of TTFMS line shapes the distortion of the diode laser modulation response appears as an asymmetry in the obtained residuals.

In the following analysis we ignore nonlinear distortion of the amplitude modulation response, since $M \ll \beta$. Including second-order nonlinear distortion, i.e., second harmonics and second-order intermodulation products, the time-dependent phase $\varphi(t)$ imposed on the laser carrier frequency can be written as

$$\varphi(t) = \beta \sin(2\pi\nu_1 t) + \beta \sin(2\pi\nu_2 t) + \zeta \sin(4\pi\nu_1 t + \vartheta) + \zeta \sin(4\pi\nu_2 t + \vartheta) + \zeta^+ \sin[2\pi(\nu_1 + \nu_2)t + \vartheta^+] + \zeta^- \sin[2\pi(\nu_1 - \nu_2)t + \vartheta^-], \tag{18}$$

where ζ and $\zeta^\pm$ are amplitudes, and ϑ and $\vartheta^\pm$ are phase shifts of the harmonics and intermodulation

products, respectively. With the previous assumption that the close spacing of the modulation frequencies ν_1 and ν_2 produces equal modulation parameters of the laser field, we also assume that equal distortion parameters are produced. By replacing the time-dependent phase shift component in the electric field in Eq. (1) with $\varphi(t)$ in Eq. (18) and also expanding the nonlinear distortion components in terms of Bessel functions, the resulting electric field can be written as

$$E(t) = E_0 \exp(i2\pi\nu_c t) \sum_n r_n \exp(i2\pi n\nu_1 t) \sum_m r_m \times \exp(i2\pi m\nu_2 t) \sum_{p=-1}^{1} J_p(\zeta)\exp[ip(4\pi\nu_1 t + \vartheta)] \times \sum_{q=-1}^{1} J_q(\zeta)\exp[iq(4\pi\nu_2 t + \vartheta)] \sum_{r=-1}^{1} J_r(\zeta^+) \times \exp\{ir[2\pi(\nu_1 + \nu_2)t + \vartheta^+]\} \sum_{s=-1}^{1} J_s(\zeta^-) \times \exp\{is[2\pi(\nu_1 - \nu_2)t + \vartheta^-]\}. \quad (19)$$

We assume that $\zeta, \zeta^{\pm} \ll \beta$, and since moderate FM indices are normally used in TTFMS, Bessel functions for the nonlinear distortion of higher than first order can be neglected. Combining the summations and approximating $J_0(\zeta) \approx J_0(\zeta^+) \approx J_0(\zeta^-) \approx 1$ we find

$$E(t) = E_0 \exp(i2\pi\nu_c t) \sum_{n,m} [(r_n + \delta_n)(r_m + \delta_m) + \delta^+_{n,m} + \delta^-_{n,m}]\exp[i2\pi(n\nu_1 + m\nu_2)t], \quad (20)$$

where

$$\delta_n(\beta, \zeta, \vartheta) \equiv J_{n-2}(\beta)J_1(\zeta)\exp(i\vartheta) + J_{n+2}(\beta)J_{-1}(\zeta)\exp(-i\vartheta), \quad (21)$$

$$\delta^{\pm}_{n,m}(\beta, \zeta^{\pm}, \vartheta^{\pm}) \equiv J_{n-1}(\beta)J_{m\mp1}(\beta)J_1(\zeta^{\pm})\exp(i\vartheta^{\pm}) + J_{n+1}(\beta)J_{m\pm1}(\beta)J_{-1}(\zeta^{\pm})\exp(-i\vartheta^{\pm}) \quad (22)$$

are due to the second-harmonic and second-order intermodulation distortion, respectively. By approximating $r_i(\beta, M, \Psi) \approx J_i(\beta)$ in all the products with distortion components and neglecting the second-order products $\delta_n\delta_m$, Eq. (20) simplifies to

$$E(t) = E_0(t) \sum_{n,m} (r_n r_m + A_{n,m})\exp[i2\pi(n\nu_1 + m\nu_2)t], \quad (23)$$

where

$$A_{n,m} \equiv J_m(\beta)\delta_n + J_n(\beta)\delta_m + \delta^+_{n,m} + \delta^-_{n,m}. \quad (24)$$

From Eq. (23) $A_{n,m}$ can be regarded as corrective terms for field sideband amplitudes. Thus, second-order nonlinear distortion can be introduced in the former theory simply by interchanging $r_n r_m$ with $r_n r_m + A_{n,m}$. When we introduce nonlinear distortion into Eq. (10a) to characterize the intensity absorption, the second-order product $A_{n,m}A^*_{n+1,m-1}$ is neglected and again the approximation $r_i(\beta, M, \Psi) \approx J_i(\beta)$ is made for all the products with distortion components. As a result, the following substitution can be used in Eq. (10a):

$$r_n r_m r^*_{n+1} r^*_{m-1} \rightarrow r_n r_m r^*_{n+1} r^*_{m-1} + J_{n+1}(\beta)J_{m-1}(\beta)A_{n,m} + J_n(\beta)J_m(\beta)A^*_{n+1,m-1}. \quad (25)$$

When introducing nonlinear distortion in relation (14) the simplified substitution

$$r_n r_m r^*_{n+1} r^*_{m-1} \rightarrow r_n r_m r^*_{n+1} r^*_{m-1} + [J_{n+1}(\beta)J_{m-1}(\beta) + J_{n-1}(\beta)J_{m+1}(\beta)]A_{n,m} \quad (26)$$

can be used.

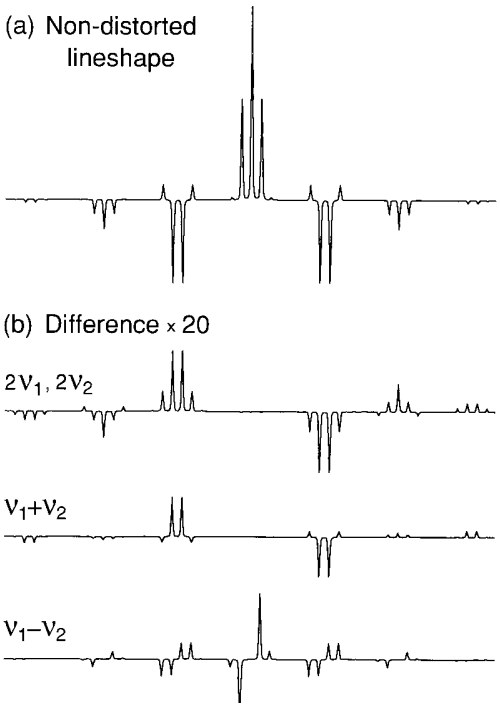

Fig. 3. (a) Theoretical nondistorted TTFMS line shape calculated for $\beta = 1.0$ and $M = 0$ and with the intermediate frequency Ω chosen larger than the absorption linewidth for illustration. (b) Differences between distorted line shapes and the nondistorted line shape in (a) showing the effect of second-harmonic and second-order intermodulation distortion at frequencies $2\nu_1$ (and $2\nu_2$) and $\nu_1 \pm \nu_2$, respectively, calculated for $\zeta, \zeta^{\pm} = 0.02$ and $\vartheta, \vartheta^{\pm} = \pi$.

Figures 3(a) and 3(b) illustrate the effect of second-harmonic and second-order intermodulation distortion, respectively, on a TTFMS line shape. Figure 3(a) is a nondistorted synthetic line shape calculated by Eq. (10a) with $\beta = 1.0$, $M = 0$, $\nu_m \gg \Delta$, and with Ω greatly exaggerated for illustration. Figure 3(b) shows the differences between line shapes subjected to second-harmonic and second-order intermodulation distortion calculated using the substitution (25) and the nondistorted line shape, respectively. The second-harmonic distortion is calculated for $\vartheta = \pi$ and $\zeta = 0.02$ ($\zeta^+, \zeta^- = 0$). The intermodulation dis-

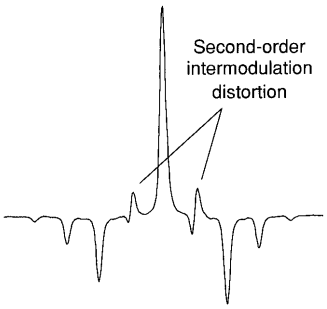

Fig. 4. Experimental TTFMS spectrum of a Fabry–Perot transmission resonance recorded with $\nu_m = 570$ MHz and $\beta \approx 1.5$. The second-order intermodulation distortion at frequency $\nu_1 - \nu_2$ is clearly visible.

tortion at frequency $\nu_1 + \nu_2$ calculated for $\vartheta^+ = \pi$ and $\zeta^+ = 0.02$ (ζ, $\zeta^- = 0$) has a similar overall asymmetrical appearance as the second-harmonic distortion. Since these two distortion components influence the line shape similarly, it is rather cumbersome to discriminate between them in practice. For ϑ, $\vartheta^\pm = 0$ the curves in Fig. 3(b) are to be inverted with respect to the zero line, and for ϑ, $\vartheta^\pm = \pm\pi/2$ the distortion does not perturb the line shape noticeably. The intermodulation distortion at frequency $\nu_1 - \nu_2$ changes only the sideband intensity distribution within a sideband group, and when $\Omega \ll \Delta$ this type of distortion has a minor influence on the line shape. However, if narrow spectral features are recorded with a large FM index β, it becomes directly observable in the spectrum, as demonstrated in Fig. 4, where a narrow-bandwidth Fabry–Perot resonance is recorded with $\beta = 1.5$, $\nu_m = 570$ MHz, and $\Omega = 10.7$ MHz. For this β a nondistorted TTFMS line shape has approximately zero amplitude at the position of the first-order sideband groups and the intermodulation distortion at frequency $\nu_1 - \nu_2$ becomes clearly observable there.

It should be noted that nonlinear distortion that may occur in the rf electronics prior to the diode laser produce harmonics and intermodulation products of the two modulating frequencies ν_1 and ν_2. If these frequencies are not prevented from reaching the diode laser they produce additional modulation of the electric field, which is described in the same way as is shown above for the distortion of the diode laser modulation response.

3. Modeling of Data

Different line profiles with varying accuracy and complexity can be used in modeling the spectral distribution of the absorbance $\alpha(\nu)$.[48] The simplest line profiles are the Gaussian produced by Doppler broadening under low-pressure conditions and the Lorentzian corresponding to collision-induced broadening under high pressure. In high-resolution measurements line shapes are often modeled as Voigt profiles. This profile is a convolution of Gaussian and Lorentzian profiles and approaches a Doppler profile at low pressure and a Lorentzian at high pressure. However, the Voigt profile deviates from recorded line shapes systematically, because of collisional (Dicke) narrowing,[20] especially if the Doppler and collisional broadening are comparable and the deviations are typically around 1%.

Collisional narrowing of line shapes arises from the reduction of the average displacement per unit time of the absorbing molecule because of velocity changing collisions, which reduces the Doppler component and changes its shape. Several refined models that include the narrowing effect have been formulated and by selecting one of these it is possible to extract line parameters with high accuracy. When the pressure-induced line shift and broadening are independent of the velocity of the absorbing molecule, the line profile is symmetrical with respect to the shifted line center. In this case the Galatry soft-collision profile[49] and the Rautian–Sobelman hard-collision profile[50] are appropriate. In the soft-collision model the velocity of a molecule after a single collision is strongly correlated with the velocity prior to the collision, whereas the hard-collision model assumes a Maxwellian velocity probability distribution after each collision. Although the velocity changing collisions in the two models are treated differently, the resulting line profiles are similar.

The line-shape functions employed in this study are normalized to the area $\sqrt{\pi}$ and standardized according to Herbert.[51] A standardized line-shape function is denoted $K(x, y, z)$, where $x \equiv (\nu - \nu_0)/\sigma$, $y \equiv \Gamma/\sigma$, and $z \equiv \xi/\sigma$. Here, $\nu - \nu_0$ is the frequency separation from the (possibly shifted) line center, σ is the Doppler halfwidth at $1/e$ intensity, Γ is the Lorentzian halfwidth at half-maximum, and ξ is the narrowing parameter. The dimensionless absorbance $\alpha(\nu - \nu_0)$ can then be expressed in terms of a standardized line profile as

$$\alpha(\nu - \nu_0) \equiv S \frac{K(x, y, z)}{\sigma \sqrt{\pi}}, \tag{27}$$

where S is the integrated line intensity defined as $S \equiv S_0 PL$, where S_0 is the line strength, P is the partial pressure of the absorbing gas, and L is the absorption path length.

The line-shape functions $K(x, y, z)$ used in our investigation are the Voigt

$$V(x, y) \equiv \frac{y}{\pi} \int_{-\infty}^{\infty} \frac{\exp(-\zeta^2)}{y^2 + (x - \zeta)^2} \, d\zeta = \mathrm{Re}[w(x, y)], \tag{28}$$

the Rautian–Sobelman

$$R(x, y, z) \equiv \mathrm{Re}\left[\frac{w(x, y + z)}{1 - \sqrt{\pi}\, z w(x, y + z)}\right], \tag{29}$$

and the Galatry

$$G(x, y, z) \equiv \frac{1}{\sqrt{\pi}} \mathrm{Re}\left(\int_0^\infty \mathrm{d}\tau \exp\left\{-ix\tau - y\tau + \frac{1}{2z^2} \times [1 - z\tau - \exp(-z\tau)]\right\}\right); \quad (30)$$

$w(x, y)$ is the complex probability function.[52] The standardized narrowing parameter is denoted z for both the Galatry and Rautian–Sobelman profiles although its physical content is somewhat different.

In the least-squares fitting procedure and when generating synthetic line shapes one can calculate the absorption component $I_\Omega{}^\alpha$ by Eq. (10a) or relation (14) and the dispersion component $I_\Omega{}^\phi$ by Eq. (10b). For simplicity the dc offset $c\varepsilon_0 E_0{}^2 M^2$ that is due to the AM can be eliminated in Eq. (10a) and relation (14) by subtraction with the nonabsorbed signal ($\alpha = 0$). The absorption of a sideband at frequency $\nu_c + n\nu_1 + m\nu_2$ can be computed according to

$$\alpha_{n,m} \equiv S \frac{K(x + n\bar{\nu}_1 + m\bar{\nu}_2, y, z)}{\sigma\sqrt{\pi}}, \quad (31)$$

where $\bar{\nu}_1 \equiv \nu_1/\sigma$ and $\bar{\nu}_2 \equiv \nu_2/\sigma$. When relation (14) is applied in the calculations we use the approximation $n\bar{\nu}_1 + m\bar{\nu}_2 \cong (n + m)\bar{\nu}_m$, where $\bar{\nu}_m \equiv \nu_m/\sigma$. Hence, the calculation of a TTFMS line shape requires five modulation parameters β, M, Ψ, $\bar{\nu}_1$, and $\bar{\nu}_2$ and five spectroscopic parameters S, y, z, ν_0, and σ. Normally, the $1/e$ Doppler halfwidth σ and the modulation frequencies $\bar{\nu}_1$ and $\bar{\nu}_2$ (or $\bar{\nu}_m$) are accurately known, and in Subsection 4.C we show that setting $\Psi = \pi/2$ is generally a good approximation for the AM–FM phase difference. Hence, the adjustable parameters to be considered in a least-squares fit are S, y, z, ν_0, β, and M.

A Levenberg–Marquardt method[53] is used for the nonlinear least-squares fitting procedure. One can calculate the real and imaginary parts of the complex probability function $w(x, y)$ using a routine by Humlicek.[54] The Galatry profile can be calculated according to Varghese and Hanson.[48] One can compute the Bessel functions using the recurrence formula

$$J_{n+1}(\beta) = \frac{2n}{\beta} J_n(\beta) - J_{n-1}(\beta), \quad (32)$$

and calculate r_n by substituting Eq. (32) into Eq. (3). Furthermore, for $\Psi = \pi/2$ the calculation of Eq. (3) simplifies to

$$r_n = J_n(\beta)\left(1 + n\frac{M}{\beta}\right). \quad (33)$$

The derivatives of the Bessel functions required in the least-squares fitting procedure are calculated as

$$J_n'(\beta) = \tfrac{1}{2}[J_{n-1}(\beta) - J_{n+1}(\beta)]. \quad (34)$$

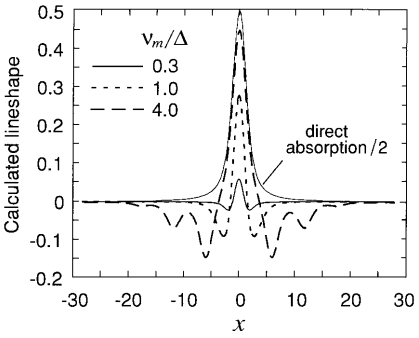

Fig. 5. Comparison of TTFMS line shapes calculated for $\nu_m/\Delta = 0.3, 1.0, 4.0$ with $y = 1.0$, $\beta = 1.0$, and $M = 0$, and the corresponding direct absorption line shape. The TTFMS line shapes are normalized to the peak amplitude of the direct absorption line shape.

The spectral fitting region is always carefully selected to be larger than the line shape extent, so effects of a limited fitting region are of no importance in this study.

We use a Voigt line-shape function in the following discussion unless otherwise stated. The Voigt HWHM Δ can be estimated from the standardized broadening parameter y used in the analysis by a simple empirical expression given by Whiting[55]:

$$\Delta/\sigma = y/2 + (y^2/4 + \ln 2)^{1/2}, \quad (35)$$

which is valid with a 1% relative error.

4. Effect of Modulation Parameters on Modeling Accuracy

A. General Consideration

Since a TTFMS line shape varies strongly with the modulation parameters, the uncertainty in a modulation parameter propagates into the spectroscopic parameters, and the magnitude of the contribution depends on the modulation parameters and the absorption width. With regard to the relative value of the modulation frequency ν_m and the absorption halfwidth Δ, two regions of interest can be distinguished, one is $\nu_m/\Delta \lesssim 1$, where the modulation parameters are strongly correlated with the spectroscopic parameters, and one is $\nu_m/\Delta \gg 1$, where sideband groups are resolved and the correlations are small. Figure 5 is a comparison of line shapes calculated for $\nu_m/\Delta = 0.3, 1.0, 4.0$ with $y = 1.0$, $\beta = 1.0$, and $M = 0$. The corresponding direct absorption line shape is also shown. For $\nu_m/\Delta \gg 1$ the absorption of a sideband group directly displays the absorption line shape, and it is possible to derive the FM and AM indices accurately from the relative peak intensities of the resolved line-shape components, the linewidth from the shape of any component, and the integrated intensity from the overall signal amplitude provided the signal is calibrated. However, in measurements of atmospheric broadened lines halfwidths are typically a few gigahertz, and since it is not simple to modulate diode lasers with frequencies in the gigahertz range

most often $\nu_m/\Delta \lesssim 1$ is the experimental reality. For this reason we emphasize this region in the following numerical investigation.

Error analysis of parameters retrieved by a least-squares fit to spectroscopic data is a complicated task.[56,57] In a straightforward approach, we investigated correlation errors by fixing one modulation parameter (β, M, or Ψ) at a time to an incorrect value in a least-squares fit to a synthetic noise-free line shape and measuring the induced errors of the adjusted parameters. In a statistical approach the retrieval accuracy can be estimated by simulating noisy spectra that are least-squares fitted with the parameters of interest adjusted.[17] Although the straightforward approach allows a wide range of modulation and line parameters to be studied efficiently by a reasonable amount of calculations, the statistical simulation is more suitable for analyzing a particular set of parameters.

A general parameter error, i.e., a deliberately generated error of a fixed parameter or an induced error of a retrieved parameter, is denoted $da \equiv a - a_t$, where a is the parameter and the subscript t indicates the true parameter value used in the synthesized line shape. The relative parameter error is denoted $\delta a \equiv (a - a_t)/a_t$. In the subsequent analysis we use the subscript t when there is the possibility of confusion. Throughout this section synthetic line shapes are calculated by relation (14) with a Voigt profile [Eq. (28)], and we often use the values $y = 1.0$ (i.e., $\Delta = 1.47\sigma$) and $\beta = 0.7$, 1.0 as the most characteristic.

B. Amplitude Modulation Index

Frequency modulation of diode lasers is always accompanied by residual amplitude modulation. The AM-to-FM index ratio M/β is an intrinsic property of a diode laser that depends on modulation frequency and bias current.[58] The residual amplitude modulation causes a line shape asymmetry, which also depends on the AM–FM phase difference. Since the AM index M and the AM–FM phase difference Ψ are closely connected in theory [Eq. (3)], it is cumbersome to determine them independently in a least-squares fit to experimental data. In a numerical approach, however, we can investigate their individual influence on the line shape and retrieval accuracy.

Figure 6(a) is a comparison of two line shapes calculated for $M = 0$ and 0.03, with $y = 1$, $S = 1$ (a.u., arbitrary unit), $\beta = 0.7$, $\Psi = \pi/2$, and $\bar{\nu}_m = 1.0$. Since the difference between the line shapes, the solid curve in Fig. 6(b), is asymmetric with respect to the line center, the determination of the line center position ν_0 is influenced by an incorrect assignment of the AM index. The dashed curve in Fig. 6(b) is the residual obtained from a least-squares fit to the asymmetric line shape using $M = 0$ and with y, S, and ν_0 adjustable. The characteristic signature of this residual is an indicator of an incorrectly determined line center position ν_0 caused by an incorrect assignment of the AM index M. The retrieved line parameters are $y = 0.998$ and $S = 0.996$, and the

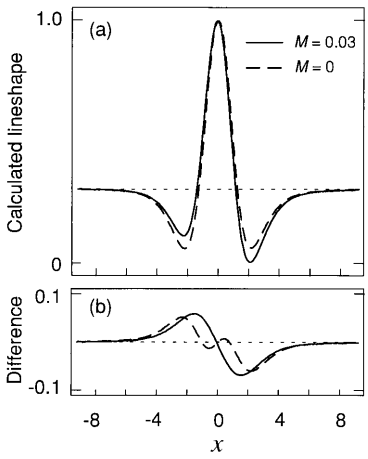

Fig. 6. (a) Comparison of TTFMS line shapes calculated for $M = 0$ (dashed curve) and $M = 0.03$ (solid curve) with $y = 1$, $\beta = 0.7$, $\Psi = \pi/2$, and $\bar{\nu}_m = 1.0$. (b) Difference (solid curve) between the two line shapes in (a) and the residual (dashed curve) obtained from a least-squares fit using $M = 0$ to the asymmetric line shape with $M = 0.03$. The scale is normalized to the TTFMS line-shape ($M = 0.03$) peak-to-peak amplitude.

normalized error of the line center determination is $d\nu_0/\sigma = -0.07$. Although the line parameters y and S are accurately determined, the line center position deviates almost one tenth of the Doppler HWHM.

The AM index-induced relative errors in the standardized broadening parameter y and the integrated line intensity S, denoted δy_M and δS_M, respectively, and the induced line center error, denoted $(d\nu_0)_M$, were determined by least-squares fits to synthetic line shapes using incorrectly fixed values of M and with y, S, and ν_0 adjustable. The synthetic line shapes were generated with different values of y, β, M, Ψ, and ν_m. By regression analysis of how δy_M and δS_M vary with each of these parameters, the following relations were found:

$$\delta y_M \cong -3.8\,\frac{\Delta}{\nu_m}\left(1 + \frac{1}{y}\right)\left(\frac{M}{\beta}\right)^2 Q_M(\delta M, \Psi),$$

$$\delta S_M \cong 1.5\,\sqrt{\frac{\Delta}{\nu_m}}\,\delta y_M \quad (0.3 < y < 3,\ 0.25 < \nu_m/\Delta < 4,\ \beta < 1.3,\ M < 0.1), \tag{36}$$

where

$$Q_M(\delta M, \Psi) \equiv [1 + \cos^2(2\Psi) + (1 + \sin\Psi)\delta M]\delta M, \tag{37}$$

which is valid for $\pi/4 \le \Psi \le 3\pi/4$ and $-1.5 < \delta M < 1$. For $\Psi = 0$, π Eq. (37) is valid with opposite sign. Relations (36) were verified for 30% validity in the specified ranges. All subsequent empirical expressions that are presented specify errors with this accuracy. It is interesting to note that both δy_M and δS_M vary quadratically with the assignment error δM and the AM–FM index ratio M/β. Figure 7 shows δy_M as a function of δM for different values of Ψ used

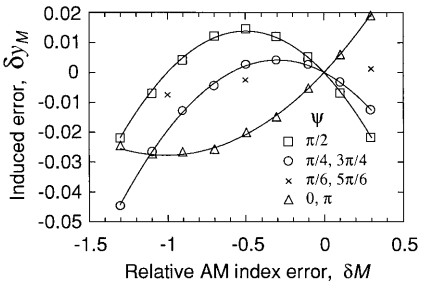

Fig. 7. Induced relative broadening error δy_M versus the relative AM index error δM. The data were obtained from least-squares fits to synthetic line shapes calculated for different Ψ with $y = 1.0$, $\beta = 1.0$, $M = 0.05$, and $\bar{\nu}_m = 1.0$. The solid curves are the induced errors that were calculated by the expressions presented in the text.

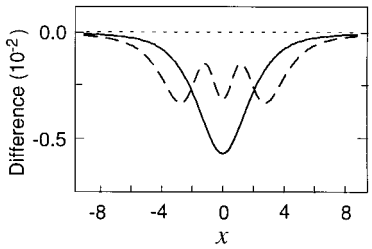

Fig. 8. Difference (solid curve) between line shapes that were calculated for $M = 0$ and 0.03, respectively, with $\Psi = \pi$, $y = 1.0$, $\beta = 1.0$, $M = 0.03$, and $\bar{\nu}_m = 1.0$, and the residual (dashed curve) obtained from a least-squares fit using $\Psi = \pi/2$ to the line shape calculated with $\Psi = \pi$ and $M = 0.03$. The scale is normalized to the TTFMS line-shape ($\Psi = \pi$) peak-to-peak amplitude.

in the fits with $S = 1$ (a.u.), $y = 1$, $\beta = 1.0$, $M = 0.05$, and $\bar{\nu}_m = 1$. The obtained errors δS_M differed only by a scale factor according to relations (36). The solid curves are calculations made by relations (36). For all the values of Ψ an underestimation of M produces more accurate line parameter values than a corresponding overestimation, and since $M = 0$ ($\delta M = -1$) induces almost no correlation errors in retrieving y and S for $\Psi = \pi/2$, this value is a good starting value in a fit. For synthetic line shapes calculated with $\Psi = \pi/6$ and $5\pi/6$, we found the correlation between the AM index and the line parameters to be negligible (Fig. 7). If the actual AM–FM phase difference Ψ is unknown and the AM index assignment error δM is moderate, boundaries of the induced line parameter errors can be calculated by relations (36) for $\Psi = \pi/2$ and π, respectively. For near-infrared diode lasers typically $M/\beta < 0.05$, and the correlation errors will be smaller than those estimated in Fig. 7.

The AM index-induced line center determination error denoted $(d\nu_0)_M$ was found to vary linearly with δM as

$$\frac{(d\nu_0)_M}{\sigma} \cong 0.6(1+y)\frac{\Delta}{\nu_m}\frac{M}{\beta}\sin\Psi\delta M \quad (0.3 < y < 3,\ 0.25 < \nu_m/\Delta < 4,\ \beta < 1.3,\ M < 0.1,\ 0 \le \Psi \le \pi). \quad (38)$$

Here the AM–FM index ratio M/β appears as the first power, and an AM index error δM influences the line center position determination more strongly than the determination of the broadening y and integrated line intensity S parameters as was demonstrated above by the result of the fit to the asymmetric line profile in Fig. 6(a). For $\Psi = 0, \pi$ the line shape is symmetrical and the determination of the line center position ν_0 exhibits no correlation with the AM index.

In a least-squares fit to experimental data the accuracy of a determination of the AM index M as an adjustable parameter is limited by the signal-to-noise ratio (SNR). Since the line-shape asymmetry is proportional to the AM index, an estimation of δM can be made from the minimum detectable asymmetry and then its contribution to the uncertainties of the measured line parameters can be calculated by relations (36) and (38) and Eq. (37).

C. AM–FM Phase Difference

In several studies with diode lasers the AM–FM phase difference Ψ was found to have a value of $\sim\pi/2$ for modulation frequencies below 750 MHz.[59,60] However, considerable deviations from $\pi/2$ have been reported for $\nu_m < 100$ MHz (Ref. 61) and $\nu_m > 750$ MHz.[59] Also variations with the laser current tuning have been observed.[12] As already mentioned, in a least-squares fit to data it is difficult to determine the AM–FM phase difference Ψ independent of AM index M. Hence a numerical investigation of how an incorrect assignment of Ψ influences the line shape and the line parameter retrieval is important.

Figure 8 shows the difference between two line shapes (solid curve) calculated for $M = 0$ and 0.03 with $y = 1$, $S = 1$ (a.u.), $\beta = 1.0$, $\Psi = \pi$, and $\bar{\nu}_m = 1$. This difference displays the effect of the residual amplitude modulation on the line shape from the imaginary part of r_n in Eq. (3) when the sideband components are unresolved. Comparison with Fig. 6(b) shows the difference with the line shape plotted for an AM–FM phase difference $\Psi = \pi/2$. The residual from a least-squares fit to the line shape calculated for $\Psi = \pi$ and $M = 0.03$, using $\Psi = \pi/2$ and with S, y, ν_0, and M adjustable, is also shown in Fig. 8 (dashed curve). The retrieved line parameters are $y = 0.99$, $S = 0.98$, $\nu_0 = (\nu_0)_t$, and $M = 0$. Residuals from fits to line shapes with other values of the FM index β and the AM index M were also obtained, and we observed that the magnitude of the residuals scales with M^2 and varies negligibly with β. From Fig. 8 it can be estimated that, if $M < 0.017$, the residual will be smaller than 10^{-3} and thus in a least-squares fit to experimental data its characteristic signature will not be resolved, and Ψ should be constrained to a reasonable value.

Synthetic line shapes with the true AM–FM phase difference Ψ_t ranging from 0 to π, were generated with various values of y, β, M, and ν_m and then fitted using an incorrectly fixed Ψ and with S, y, ν_0, and M

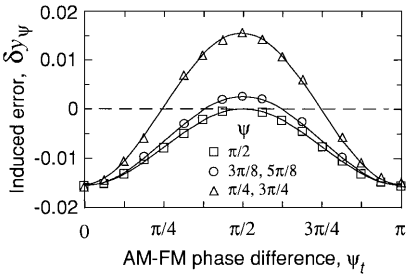

Fig. 9. Induced relative broadening error δy_Ψ versus the AM–FM phase difference Ψ_t. The error δy_Ψ was obtained from least-squares fits using differently fixed Ψ to synthetic line shapes calculated for different Ψ_t with $y = 1.0$, $\beta = 1.0$, $M = 0.05$, and $\bar{\nu}_m = 1.0$. The solid curves represent the induced errors that were calculated by the expressions presented in the text.

adjustable. By analyzing how the relative errors δy_Ψ and δS_Ψ induced by the AM–FM phase difference vary with each of y, β, M, Ψ_t, and ν_m, we found the expressions

$$\delta y_\Psi \cong 2.1 \frac{\Delta}{\nu_m}\left(1 + \frac{1}{y}\right)\left(\frac{M}{\beta}\right)^2 Q_\Psi(\Psi, \Psi_t),$$

$$\delta S_\Psi \cong 1.5 \sqrt{\frac{\Delta}{\nu_m}}\, \delta y_\Psi \quad (0.3 < y < 3,\ 0.25 < \nu_m/\Delta < 4,\ \beta < 1.3,\ M < 0.1), \tag{39}$$

where

$$Q_\Psi(\Psi, \Psi_t) \equiv \left(\frac{\sin \Psi_t}{\sin \Psi}\right)^2 - 1 \quad (\pi/8 \le \Psi \le 7\pi/8). \tag{40}$$

The similarity of relations (39) and (36) demonstrates the connection between the AM index M and the AM–FM phase difference Ψ in the theory. Figure 9 shows δy_Ψ as a function of Ψ_t for different values of Ψ used in the least-squares fits and $y = 1$, $S = 1$ (a.u.), $\beta = 1.0$, $M = 0.05$, $\bar{\nu}_m = 1$. The obtained errors δS_Ψ differed only by a scale factor according to relations (39). The solid curves are calculations by relations (39). Since the variation of the induced relative broadening error δy_Ψ is minimal for $\Psi = \pi/2$, it is advantageous to adopt this value when the actual value of Ψ is unknown. The systematic correlation errors hereby introduced in the line parameter determination are always negative, and the error boundaries can be estimated by setting $\Psi_t = 0$ or π in relations (39). Then the retrieved line parameter values can be corrected by as much as half of the corresponding error boundary. It should be noted that the fitted values of the AM index M follow the expected relation $M \sin \Psi = M_t \sin \Psi_t$, whereas the determination of the line center position ν_0 is not affected. Thus, we conclude that $\Psi = \pi/2$ is generally a good approximation for the AM–FM phase difference.

D. Frequency Modulation Index

The influence of the assignment of the FM index β on the retrieval accuracy of the least-squares fitted parameters varies with the choice of β and ν_m/Δ. In the $\nu_m/\Delta \lesssim 1$ region in particular the FM index correlates significantly with the broadening parameter y and the integrated line intensity S. The FM index was not found to correlate with ν_0, M, and Ψ, and in the following analysis we set $M = 0$ for simplicity.

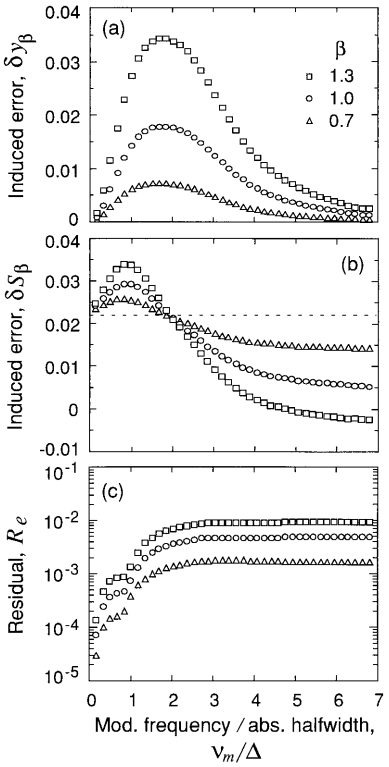

Fig. 10. (a) Induced relative broadening parameter error δy_β, (b) induced relative integrated line intensity error δS_β, (c) amplitude of the residuals R_e as functions of ν_m/Δ. The data were obtained from least-squares fits where $\delta\beta = -0.1$ to synthetic line shapes calculated for $\beta = 0.7$, 1.0, 1.3 with $y = 1.0$ ($\Delta = 1.47\sigma$) and $M = 0$.

To evaluate the correlation-induced errors in the line parameter retrieval as a function of ν_m/Δ, we generated synthetic line shapes with ν_m/Δ ranging from 0.1 to 10 ($y = 1.0$) and least-squares fitted them using $\beta = 0.9\beta_t$ (i.e., $\delta\beta = -0.1$) with y and S adjustable. Figure 10 shows plots of the FM index-induced relative line parameter errors denoted δy_β, and δS_β, and the peak-to-peak amplitude R_e of the residuals normalized to the synthetic line shape peak-to-peak amplitude versus ν_m/Δ, respectively, for $\beta = 0.7$, 1.0, 1.3. Figure 10(a) shows that the largest broadening error δy_β occurs when the modulation frequency ν_m matches the linewidth 2Δ of the absorbing feature and that the induced error is strongly dependent on the FM index. The largest induced integrated line intensity error δS_β occurs when the modulation frequency matches the halfwidth Δ [Fig. 10(b)]. When the modulation frequency is nearly the same as the linewidth, δS_β is independent of the FM index, and for larger modulation frequencies δS_β decreases with increasing FM index. Note how the correlation error δS_β for large β varies strongly with ν_m/Δ and for small β approaches a constant value (dashed line).

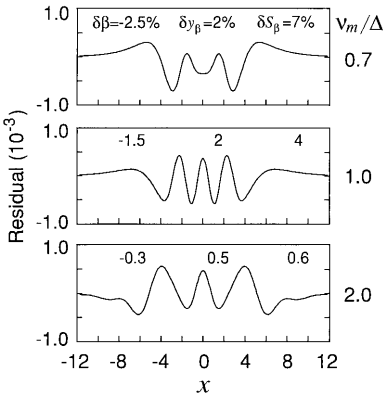

Fig. 11. Residuals that were obtained from least-squares fits using incorrectly assigned FM indices to synthetic line shapes calculated for $\nu_m/\Delta = 0.7, 1.0, 2.0$ with $y = 1.0$, $\beta = 1.0$, and $M = 0$. The scales are normalized to the corresponding line-shape peak-to-peak amplitude ($R_e = 10^{-3}$). Above each plot is the corresponding FM index error $\delta\beta$ and the induced errors δy_β and δS_β.

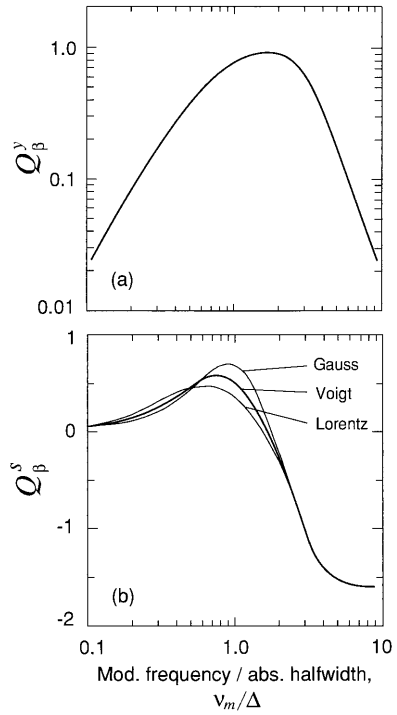

Fig. 12. Coefficients (a) $Q_\beta{}^y$ and (b) $Q_\beta{}^S$ versus ν_m/Δ that were used in the expressions presented in the text to calculate FM index-induced errors in the retrieved broadening and integrated line intensity parameters. The coefficient $Q_\beta{}^S$ was plotted for Gaussian ($y = 0$), Lorentzian ($y = \infty$), and Voigt ($y = 1.0$) profiles.

Figure 10(c) in turn can be regarded as the sensitivity of the fitted line shape to an incorrect assignment $\delta\beta$ of the FM index as a function of ν_m/Δ. This means that, for a particular SNR, choosing a modulation frequency for which $\nu_m/\Delta > 2$ the FM index can be determined with approximately 1 order of magnitude higher accuracy than in the $\nu_m/\Delta \leq 1$ region.

A conceptual understanding of the results presented in Fig. 10 can be acquired using Fig. 5, where line shapes for $\nu_m/\Delta = 0.3, 1.0, 4.0$ were illustrated. For small values of ν_m/Δ the amplitudes scale with ν_m without significant line-shape change. At modulation frequencies ν_m comparable with the absorption halfwidth Δ the absorption of individual sideband groups becomes resolved. We resolved the sideband components for high modulation frequencies, which has the result that the line shape broadens proportionally with ν_m without a change of amplitude. In this region with resolved sideband groups, the magnitude of the correlations in the least-squares fit between the FM index and the line parameters is reduced.

Figure 11 shows a comparison of the residuals obtained for $\nu_m/\Delta = 0.7, 1.0, 2.0$ and $\beta = 1.0$ with the FM index error $\delta\beta$ chosen such that $R_e = 10^{-3}$. The corresponding assignment error $\delta\beta$ of the FM index and the induced line parameter errors δy_β and δS_β are presented in the figure. The characteristic signatures of these residuals can be used in the modeling of experimental data to trace an incorrectly assigned FM index.

For a more general evaluation of how the FM index-induced line parameter errors δy_β and δS_β depend on the choice of y, β, and ν_m, synthetic line shapes were generated over a wide parameter range and fitted again using an FM index fixed incorrectly near the true value and with y and S adjustable. By regression analysis of how δy_β and δS_β depend on each y, β, and ν_m, expressions valid for $\nu_m/\Delta > 0.1$, $\beta < 1.4$, and $|\delta\beta| < 0.3$ could be formulated:

$$\delta y_\beta \cong -Q_\beta{}^y\left(1 + \frac{1}{y}\right)\beta^{2.5}\delta\beta, \tag{41}$$

$$\delta S_\beta \cong -(2.2 + Q_\beta{}^S\beta^{1.5})\delta\beta, \tag{42}$$

where the coefficients $Q_\beta{}^y$ and $Q_\beta{}^S$ depend on the ratio of ν_m/Δ. Relation (41) has the additional condition of $y > 0.1$. In Fig. 12 we plotted the coefficients (a) $Q_\beta{}^y$ and (b) $Q_\beta{}^S$ as a function of ν_m/Δ. The coefficient $Q_\beta{}^S$ is slightly dependent on the value of y and is plotted for Gaussian ($y = 0$), Voigt ($y = 1.0$), and Lorentzian ($y = \infty$) line profiles. The FM index-induced integrated line intensity error δS_β depends most on the line profile when the modulation frequency ν_m coincides with the absorption halfwidth Δ. For small values of β or ν_m/Δ, relation (42) reduces to $\delta S_\beta \approx -2\delta\beta$. The relative broadening error δy_β depends strongly on the FM index β and always has opposite sign with respect to the assignment error $\delta\beta$. For a known uncertainty of the FM index the induced relative errors δy_β and δS_β can be estimated by relations (41) and (42) for different experimental configurations.

In contrast to the AM index and AM–FM phase difference-induced line parameter errors, the FM index-induced errors δy_β and δS_β and magnitude R_e of the residuals are linearly proportional to the FM index assignment error $\delta\beta$. Therefore, the data in Fig. 10 can be used to calculate the induced errors at an

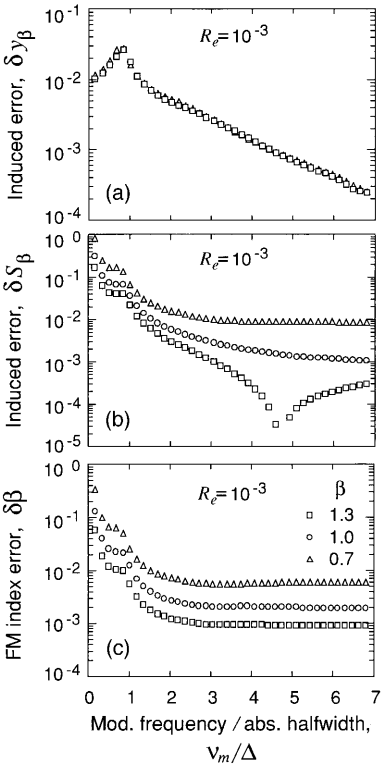

Fig. 13. (a) Induced broadening error δy_β, (b) induced integrated intensity error δS_β, (c) FM index error $\delta\beta$ as functions of ν_m/Δ calculated for a magnitude of the residuals of 10^{-3} from the data presented in Fig. 10.

arbitrary magnitude R_e of the residual. For a spectroscopic device with an instrumental distortion of a particular magnitude (or noise level) the numerically calculated line parameter errors δy_β and δS_β can be taken as error boundaries that are introduced in the line-shape measurement. Figure 13 shows calculations of the induced line parameter errors (a) δy_β and (b) δS_β and (c) the FM index error $\delta\beta$ as functions of ν_m/Δ for $R_e = 10^{-3}$, which corresponds to the lowest instrumental distortions currently achievable. Since a sign assignment is normally not possible in modeling experimental data, all the presented values are positive. The largest correlation error in retrieving the broadening parameter y occurs around $\nu_m/\Delta = 0.75$. It is noteworthy that the FM index-induced broadening error δy_β for a specific magnitude of residual errors R_e is independent of the value of β. The correlation error δS_β in retrieving the integrated line intensity reduces with the FM index and ν_m/Δ, and for some specially chosen modulation parameters it is zero, e.g., for $\beta = 1.3$ and $\nu_m/\Delta \approx 4.7$. The main reduction of the FM index retrieval error $\delta\beta$ and the induced line parameter errors δy_β and δS_β occurs in the $0.8 < \nu_m/\Delta < 2$ region. The experimental uncertainty of a least-squares fitted FM index can be estimated from Fig. 13(c) for an arbitrary value of β and noise level by using the approximate relation $\delta\beta \propto R_e/\beta^{2.5}$, which was found by fits to line shapes generated with different values of y and β. Then the FM index-induced line parameter uncertainties δy_β and δS_β can be calculated by relations (41) and (42).

For spectra in which the SNR is limited by random noise, e.g., laser source noise and detector shot noise, the uncertainty of the retrieved parameters can be estimated by statistical simulations.[57] Multiple sets of random noise with a normal (Gaussian) distribution were generated and added to a synthetic line shape calculated with $y = 1.0$, $\nu_m/\Delta = 1.0$, and $\beta = 1.0$. In the least-squares fits y, S, and β were adjustable, and the fitting region was $\pm 5\Delta$ with a total number of 150 data points. Fits with the FM index β fixed to the true value were also performed. The results are summarized in Table 1, where the standard deviations and systematic errors (bias) of the retrieved parameters are presented for SNR's of 50, 100, and 400. Linear correlation coefficients for the retrieved parameters were calculated and are also presented. The retrieved parameters were not sensitive to their starting values.

The results in Table 1 show that the standard deviations of the line parameters (σ_y, σ_S) increase significantly when the FM index β is released in the least-squares fitting procedure. Again, a strong correlation between the FM index and the line parameters appears, which is also confirmed by the linear correlation coefficients that indicate a nearly complete negative correlation. Thus, the random noise causes an error in the fitted FM index, which propa-

Table 1. Results from Least-Squares Fits to Synthetic Data with Random Noise

SNR[a]	Standard Deviation (%)			Systematic Error (%)			Correlation Coefficient			Data Sets
	σ_y	σ_S	σ_β	δy	δS	$\delta\beta$	$C_{y,\beta}$	$C_{S,\beta}$	$C_{y,S}$	
					β Fitted					
50	6	9	3.5	−4	−6	2	−0.92	−0.95	0.99	100
100	5	8	3.5	−0.3	−0.4	0.2	−0.96	−0.98	0.99	200
400	2.5	4	1.5	0.2	0.3	−0.1	−1.0	−1.0	1.0	100
					β Fixed to the True Value					
50	2	2.5	—	−1	−1.4	—	—	—	0.98	50
100	1.5	2	—	−0.8	−0.6	—	—	—	0.98	50
400	1	1.5	—	−0.3	−0.4	—	—	—	0.98	50

[a]SNR is defined as the ratio of the line shape peak-to-peak amplitude to the noise rms value.

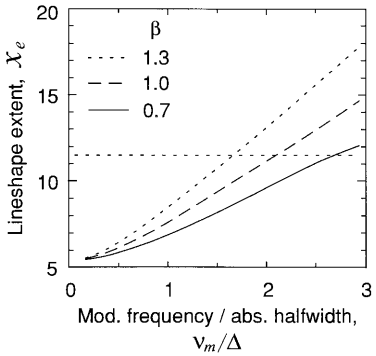

Fig. 14. Line-shape extent X_e, defined as the standardized halfwidth at 0.01 of the line-shape peak-to-peak value, as a function of ν_m/Δ calculated for $\beta = 0.7, 1.0, 1.3$ with $y = 1.0$ and $M = 0$. The corresponding extent of the direct absorption line shape is indicated by the horizontal dashed line.

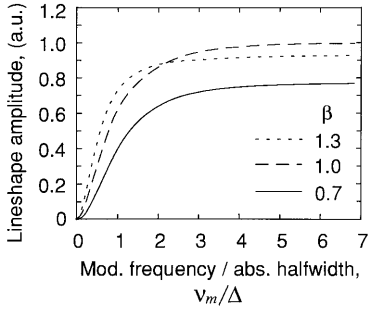

Fig. 15. TTFMS line-shape peak-to-peak amplitude versus ν_m/Δ calculated for $\beta = 0.7, 1.0, 1.3$ with $y = 1.0$ and $M = 0$.

gates into the retrieval of the line parameters. These correlations are in agreement with the previous analysis, and the standard deviations of the retrieved parameters follow relations (41) and (42). The standard deviations obtained for a SNR of 400 correspond to the parameter errors of $|\delta y_\beta| = 0.02$, $|\delta S_\beta| = 0.04$, and $|\delta\beta| = 0.015$ estimated for the residual amplitude of 10^{-3} from Figs. 11 and 13. Note that the parameters retrieved from data with a SNR of 50 show noticeable systematic errors, which should be considered when modeling noisy line shapes. Also, the systematic errors obtained satisfy relations (41) and (42).

E. Optimum Choice of Modulation Frequency and FM Index

As the previous analysis has shown, the choices of FM index β and modulation frequency ν_m relative to the absorption halfwidth Δ significantly influence the retrieval accuracy of the line parameters. When one optimizes the modulation parameters it is desirable that the outcome involves small FM index-induced line parameter errors as well as high sensitivity and selectivity. This implies large line-shape amplitude and narrow spectral extent. The least-squares fitting results presented in Fig. 13 indicate that choices of the FM index as large as possible and the modulation frequency larger than the linewidth 2Δ yields small correlation errors. However, the large spectral interval occupied by the line shape at high modulation frequencies is a disadvantage because of the wide tuning range required to record the line shape and the possible overlap with other lines, e.g., in Fig. 5 the line shape calculated with $\nu_m/\Delta = 4$ ranges over $x \approx \pm 20$, which is nearly 15 times the linewidth of the absorbing feature. If the selectivity is crucial, a reduction of the modulation frequency below the absorption linewidth becomes advantageous, since the TTFMS line-shape extent for moderate FM indices will be even smaller than the extent of the corresponding direct detected line shape. Figure 14 shows calculations of the TTFMS line-shape extent X_e, defined as the standardized halfwidth at 0.01 of the line-shape peak-to-peak value, as a function of ν_m/Δ for $\beta = 0.7, 1.0, 1.3$ with $y = 1.0$. The corresponding extent of the direct absorption line shape is indicated by a horizontal dashed line, and hence, for $\nu_m \lesssim 2\Delta$, the extent of the TTFMS line shape is smaller than for the direct detected absorption and it is further reduced with a lower FM index.

The line-shape amplitude scales with the FM index. Figure 15 shows the line-shape peak-to-peak amplitude calculated using relation (14) for $\beta = 0.7, 1.0, 1.3$ as a function of ν_m/Δ with $y = 1.0$. For $\nu_m/\Delta > 2$ we found that the line-shape amplitude maximizes at $\beta = 1.03$, which is in agreement with Ref. 31. Increasing the FM index further decreases the line-shape amplitude and widens the spectral extent. Moreover, at large FM indices the nonlinear distortion of the laser modulation response may alter the line shape significantly (Fig. 4).

In practice, the accessible range of the modulation parameters can be determined by the capability of the modulation scheme and spectrum of interest. Nevertheless, a preferable choice is a modulation frequency comparable with or larger than the linewidth, provided that overlapping with other lines is avoided, and an FM index of ~ 1. Then for a recorded line shape with the selected experimental configuration, the accuracy with which the FM index has to be adjusted in the least-squares fit, in order to reduce the induced correlation errors in the fitted line parameter to a desired uncertainty level, can be estimated by relations (41) and (42).

Since the accuracy in the assignment of the FM index plays a key role in the retrieval of the line parameters, it is advisable to measure it separately and fix it in the least-squares fitting procedure. In Ref. 43 we demonstrated a method with which the FM index can be determined with improved accuracy. The method was based on multiple fittings of three spectra recorded with different unknown FM indices. Again, if the resulting accuracy is known the induced line parameter uncertainties can be estimated by relations (41) and (42).

5. Dispersion

As already discussed in Section 2, if the heterodyne detection phase θ is adjusted for the optimum signal, there is a contribution from dispersion in the signal.

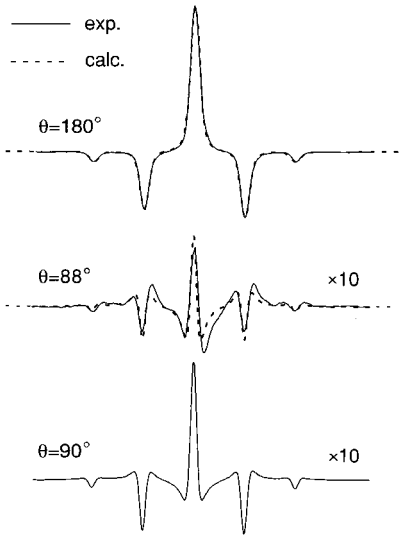

Fig. 16. Comparison of experimental TTFMS spectra of a Fabry–Perot transmission resonance recorded with phase-sensitive detection at $\theta = 180°$ and 88° and corresponding theoretical line shapes. A dispersion line shape calculated for $\theta = 90°$ is also illustrated. The diode laser was frequency modulated at 570 ± 5.4 MHz with $\beta = 0.7$ and $M = 0.01$.

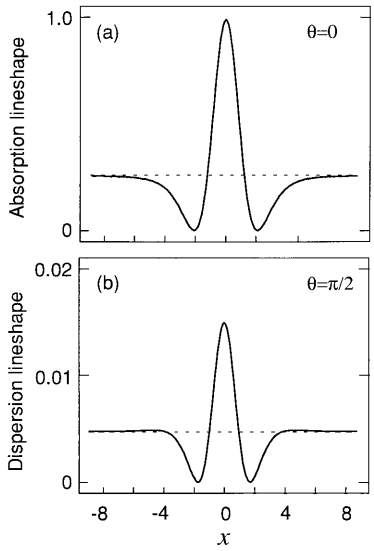

Fig. 17. Comparison of theoretical (a) absorption and (b) dispersion line shapes that were calculated using a Voigt profile with $y = 1$, $\beta = 1.0$, $M = 0$, $\bar{\nu}_m = 1$, and $\Omega = 0.02\sigma$.

Moreover, since a precise adjustment of the detection phase in many cases is not simple to accomplish, it is necessary to consider the dispersion component carefully.

To examine dispersion from a narrow width spectral feature for which $\nu_m/\Delta \gg 1$, we scanned the laser wavelength through a Fabry–Perot resonance. Figure 16 shows the experimental TTFMS line shapes with the detection phase adjusted for an optimum signal ($\theta \approx 180°$) and with the detection phase shifted approximately 90°. The line shapes were recorded with $\nu_m = 570$ MHz, $\Omega = 10.8$ MHz. Figure 16 also shows the corresponding theoretical line shapes that we calculated by substituting Eqs. (10a) and (10b) into relation (13) with $\theta = 180°$ and $\theta = 88°$, respectively, and $\beta = 0.7$ and $M = 0.01$. The calculated line shapes agree well with the experimental results although the Fabry–Perot transmission function for simplicity was calculated using a Voigt profile and the approximation in Eq. (8) is not appropriate. The asymmetry of the line shapes originates from an asymmetrical Fabry–Perot apparatus function that is due to a misalignment to reduce optical feedback into the diode laser. As seen, the dispersion component is as large as 8% of the quadrature component and caution is advisable when one measures narrow line shapes. For demonstration, a calculated pure dispersion line shape ($\theta = 90°$) is also shown in Fig. 16.

Since the TTFMS dispersion line shape is similar to the second derivative of the absorption line shape (quadrature), we expect that the contribution of dispersion influences only the retrieval of the broadening parameter y. Figures 17(a) and 17(b) compare the pure absorption and dispersion line shapes calculated by Eqs. (10a) and (10b) for $\nu_m/\Delta = 1.47$ using a Voigt profile (with $y = 1$, $\beta = 1.0$, $M = 0$, $\bar{\nu}_m = 1$, and $\Omega = 0.02\sigma$). These line shapes were used to synthesize two line shapes according to relation (13) with $\theta = \pm 45°$, both of which were least-squares fitted by a pure absorption line shape ($\theta = 0$) with y, S, and β adjustable. Although the retrieved integrated line intensity S and the FM index β were not noticeably affected, the dispersion-induced error in the broadening parameter was $\delta y_\phi = \mp 0.01$ (for $\theta = \pm 45°$), and although the dispersion was nearly 2% of the absorption the obtained residual was as small as $R_e \approx 10^{-4}$. This means that it is not possible to detect a dispersion component in the heterodyne signal by a least-squares fit to experimental data. Since it might induce a significant error in the broadening parameter retrieved, the detection phase should be adjusted as accurately as possible to the absorption signal.

Numerical modeling was performed to evaluate how the dispersion component $I_\Omega{}^\phi$ varies with the modulation parameters (β, ν_m, Ω) and the width of the spectral feature. The peak-to-peak values of the pure dispersion and absorption components as functions of β, Ω, and ν_m/Δ were determined using Eqs. (10a) and (10b). Figure 18 shows plots of $(I_\Omega{}^\phi)_{pp}/(I_\Omega{}^\alpha)_{pp}$ normalized to Ω/Δ versus ν_m/Δ for Gaussian ($y = 0$), Voigt ($y = 1.0$), and Lorentzian ($y = \infty$) line profiles. For $\nu_m/\Delta > 3$, the normalized ratio is ~0.5, and for $\nu_m/\Delta < 3$ it increases with decreasing ν_m/Δ and is more dependent on the line profile. Additionally, the ratio was found to be independent of the value of β, and thus Fig. 18 can be used to estimate the magnitude of a heterodyne-detected dispersion component relative to the absorption for an arbitrary experimental configuration.

6. Collisional Narrowing

One can often use a Voigt profile in modeling data because of its computational simplicity. If the ex-

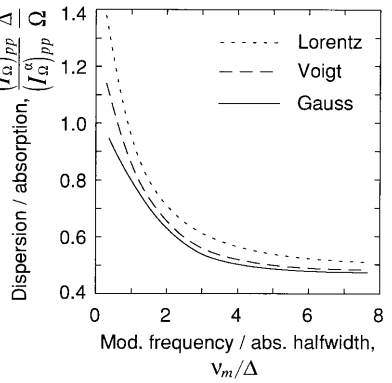

Fig. 18. Ratio of the dispersion $(I_\Omega{}^\phi)_{pp}$ and absorption $(I_\Omega{}^\alpha)_{pp}$ intensity components normalized to Ω/Δ versus ν_m/Δ. The data were obtained from synthetic TTFMS line shapes that were calculated using Gaussian ($y = 0$), Lorentzian ($y = \infty$), and Voigt ($y = 1.0$) profiles.

perimental condition is such that collisional narrowing is significant, a more elaborate line profile yields line parameters with improved accuracy. For this reason it is of interest to specify a characteristic signature in the residual from a least-squares fit to a collisionally narrowed line shape when one uses a Voigt profile.

Figure 19(a) shows a synthetic line shape that was generated with a Galatry profile [with $y = 1$, $S = 1$ (a.u.), $z = 1$, $\beta = 0.7$, $M = 0$, and $\bar{\nu}_m = 1$], and the residuals from least-squares fits to it when we used a Voigt and a Rautian–Sobelman profile. The fitted line parameters are $y = 0.65$, $S = 0.76$ for the Voigt profile and $y = 0.97$, $S = 0.985$, $z = 0.75$ for the Rautian–Sobelman profile. Although the Rautian–Sobelman profile fits the data to better than 0.2%, the residual from the Voigt fit is approximately 6%. Figure 19(b) shows the corresponding direct absorption line shape and the residuals that were obtained with the same least-squares fitting procedure with the same line parameters as above. The best-fit parameters are $y = 0.88$, $S = 0.97$ for the Voigt profile and $y = 0.99$, $S = 0.999$, $z = 0.85$ for the Rautian–Sobelman profile. The characteristic signature and the magnitude of the residuals agree with the result presented in Ref. 48. Although the magnitudes of the residuals from the least-squares fits to the TTFMS and the direct absorption line shapes are comparable, the parameters retrieved from TTFMS line shapes show a larger variation with the choice of line profile. Hence, if a Voigt profile is used in a least-squares fit to a collisionally narrowed TTFMS line shape, there might be significant systematic errors in the retrieved line parameters. Since the difference between the Galatry and the Rautian–Sobelman profiles in the fit is at a level that is normally smaller than the experimental precision, the choice between them is more a matter of convenience.

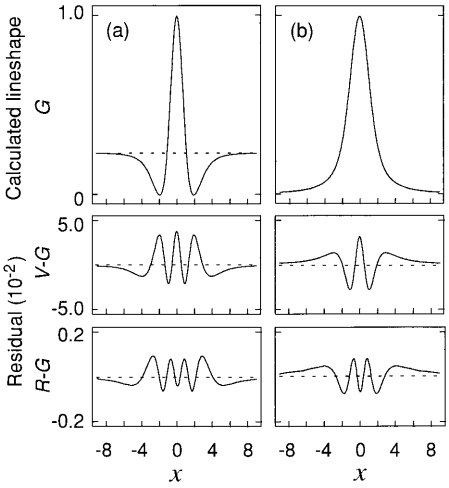

Fig. 19. (a) TTFMS line shape calculated with a Galatry profile (G) for $y = 1$, $z = 1$, $\beta = 0.7$, $M = 0$, and $\bar{\nu}_m = 1$, and the residuals that were obtained from a least-squares fit using Voigt (V) and Rautian–Sobelman (R) profiles. (b) Corresponding direct absorption line shape and residuals.

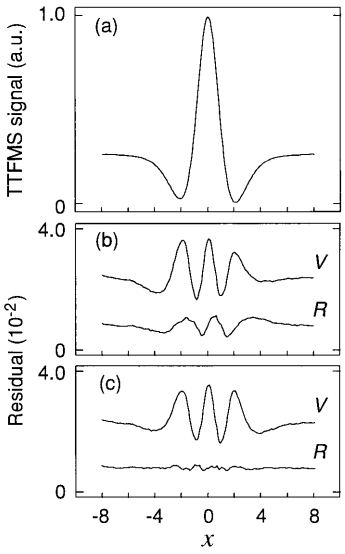

Fig. 20. Comparison of the results from least-squares fits to experimental data. (a) TTFMS recording of the R15Q16 oxygen transition at a total pressure of 200 Torr. (b) Residuals from a fit using Voigt (V) and Rautian–Sobelman (R) profiles. (c) Residual obtained when second-harmonic distortion is included in the TTFMS theory. The curves are offset for clarity.

7. Experimental Data

Figure 20(a) shows a spectrum of the oxygen R15Q16 line at 13,156 cm^{-1}, recorded with $\nu_m = 585$ MHz and $\Omega = 10.7$ MHz. The oxygen cell pressure was 200 Torr, giving a peak absorption of 4.7% and a HWHM of $\Delta \approx 650$ MHz. The linearity of the data acquisition system was approximately 0.1%. The detection phase was adjusted with a precision of $\pm 5°$, and, since Fig. 18 gives $(I_\Omega{}^\phi)_{pp} \approx 0.016(I_\Omega{}^\alpha)_{pp}$, the heterodyne-detected dispersion component is less than 1.4×10^{-3} of the absorption component and is thus negligible. The upper trace in Fig. 20(b) is the residual from a least-squares fit that was obtained us-

ing Eq. (10a) with a Voigt profile and $\Psi = \pi/2$, which provided the best-fit parameters $y = 0.62$, $S = 1.0$ (a.u.), $\beta = 0.90$, and $M = 0.0051$. The characteristic signature of the residual reveals the presence of collisional narrowing [Fig. 19(a)]. The lower trace in Fig. 20(b) is the residual from a Rautian–Sobelman fit, which provided the best-fit parameters $y = 0.70$, $S = 1.07$ (a.u.), and $z = 0.13$, $\beta = 0.89$, and $M = 0.0053$.

The asymmetry of the residuals in Fig. 20(b) originates from nonlinear distortion of the diode laser modulation response. We carefully checked to ensure that a signal distortion of this shape and magnitude was not produced by the detection scheme. Furthermore, since the oxygen self-shift is much smaller than the self-broadening, the oxygen line should be properly described by the employed symmetrical line profile.[21] Figure 20(c) shows the residuals from refits to the experimental data, for which second-harmonic distortion was accounted for by introducing substitution (25) into Eq. (10a) with $\vartheta = \pi$. By fixing the distortion parameter ζ differently, whereas the same parameters as in the previous fits are adjustable, a best fit was obtained for $\zeta = 0.015$. The Voigt fit now produces a symmetrical residual and the residual from the collisionally narrowed line profile is significantly reduced showing no clear characteristic deviations. The retrieved line parameters were not noticeably affected in this case with small distortion, nevertheless, inclusion of nonlinear distortion in the theory greatly improves the fitting quality and permits other discrepancies between model and experiment to be observed.

The magnitude of the residual from the Rautian–Sobelman fit in Fig. 20(c) is $\sim 2 \times 10^{-3}$. From Fig. 13(c) we estimate that this magnitude yields an uncertainty $\delta\beta \approx 0.025$ of the fitted FM index, and with relations (41) and (42) we calculated the corresponding line parameter uncertainties as $\delta y_\beta \approx 0.03$ and $\delta S_\beta \approx 0.07$. To estimate the line parameter uncertainties induced by the approximation $\Psi = \pi/2$, we assume an unfavorable value of the true AM–FM phase difference, such as $\Psi_t = 7\pi/8$ for which the true AM index is $M_t = M/\sin \Psi_t \approx 0.013$; then with relations (39) and Eq. (40) we obtain $\delta y_\Psi \approx -0.001$ and $\delta S_\Psi \approx -0.0016$. The uncertainty in the fitted AM index M can be estimated from the ratio of the residual amplitude and the line-shape asymmetry to $|\delta M| \approx 0.07$, and with relations (36) and Eq. (37) we calculated the AM index-induced uncertainties to be approximately 2 orders of magnitude smaller than the FM index-induced line parameter uncertainties. Thus, the uncertainties induced by an incorrect assignment of the AM–FM phase difference Ψ and the AM index M are negligible in comparison with those induced by the FM index β.

8. Conclusion

By accounting for dispersion and nonlinear distortion of the frequency modulation response of diode lasers, a TTFMS theory was derived that is applicable to model line shapes over a wide range of modulation and line parameters. By using a least-squares fitting procedure to model numerically generated TTFMS line shapes we evaluated and specified the correlation of modulation and line parameters over a wide range of parameters. From the acquired numerical data we derived empirical expressions that specify the errors in retrieving the broadening and the integrated line intensity parameters that are due to incorrect assignments of the modulation parameters. Since the uncertainty in the assignment of the FM index is the main source of correlation error in retrieving these line parameters, it is strongly recommended that this parameter be assigned accurately prior to a fit. The correlations of the AM index and the AM–FM phase difference with the line parameters are negligible unless the residual amplitude modulation is large. An error in the assignment of the AM index propagates mainly into the line center position retrieval.

It was shown that, depending on the heterodyne detection phase and the choice of detection frequency relative to the measured linewidth, dispersion may contribute significantly to a recorded line shape. Since the dispersion contribution introduces an error of the retrieved broadening parameter, careful adjustment of the heterodyne detection phase is necessary. The nonlinear distortion of the modulation response was shown to result in an asymmetrical distortion of the line shape, which may be severe at large FM indices or abnormal operation conditions of the diode laser.

The least-squares fits to experimental TTFMS data of a collisionally broadened oxygen line using Voigt and Rautian–Sobelman line profiles confirmed the validity of the numerical investigation. Systematic discrepancies in the residual (observed–calculated) obtained from the fit using a Voigt profile displayed a clear influence of collisional (Dicke) narrowing that was in good agreement with calculated residuals. By refitting the data using a collisionally narrowed Rautian–Sobelman profile and by correcting for the second-harmonic distortion we demonstrated discrepancies smaller than 2×10^{-3}. Although the retrieved parameters were not noticeably affected when we accounted for the nonlinear distortion, this significantly improved the fitting quality.

This study has shown that, by an appropriate choice of modulation parameters, accurate determination of line parameters of transitions recorded by TTFMS is possible. This implies that accurate quantitative measurements over a wide range of concentrations, temperatures, and pressures can be performed with high sensitivity by TTFMS.

We gratefully acknowledge Sune Svanberg for support and Ulf Gustafsson for valuable suggestions on the manuscript. This study was supported by the Swedish Research Council for Engineering Science and the Swedish Board for Industrial and Technical Development.

References

1. A. C. Stanton and J. A. Silver, "Measurements in the HCl 3–0 band using a near-IR InGaAsP diode laser," Appl. Opt. **27,** 5009–5015 (1988).
2. C. B. Carlisle, H. Riris, L.-G. Wang, G. R. Janik, T. F. Gallagher, A. L. Pineiro, and R. H. Tipping, "Measurement of high overtone intensities of HBr by two-tone frequency-modulation spectroscopy," J. Mol. Spectrosc. **130,** 395–406 (1988).
3. C. B. Carlisle and D. E. Cooper, "Tunable diode laser frequency modulation spectroscopy through an optical fiber: high sensitivity detection of water vapor," Appl. Phys. Lett. **56,** 805–807 (1990).
4. H. Riris, C. B. Carlisle, D. E. Cooper, L. Wang, T. F. Gallagher, and R. H. Tipping, "Measurement of the strengths of 1–0 and 3–0 transitions of HI using frequency modulation spectroscopy," J. Mol. Spectrosc. **146,** 381–388 (1991).
5. T. J. Johnson, F. G. Wienhold, J. P. Burrows, and G. W. Harris, "Frequency modulation spectroscopy at 1.3 μm using InGaAsP lasers: a prototype field instrument for atmospheric chemistry research," Appl. Opt. **30,** 407–413 (1991).
6. P. Kauranen, I. Harwigsson, and B. Jönsson, "Relative vapor pressure measurements using a frequency modulated tunable diode laser, a tool for water activity determination in solutions," J. Phys. Chem. **98,** 1411–1415 (1994).
7. P. Kauranen, H. M. Hertz, and S. Svanberg, "Tomographic imaging of fluid flows by the use of two-tone frequency-modulation spectroscopy," Opt. Lett. **19,** 1489–1491 (1994).
8. H. Riris, C. B. Carlisle, L. W. Carr, D. E. Cooper, R. U. Martinelli, and R. J. Menna, "Design of an open path near-infrared diode laser sensor: application to oxygen, water, and carbon dioxide vapor detection," Appl. Opt. **33,** 7059–7066 (1994).
9. L. S. Rothman, R. R. Gamache, R. H. Tipping, C. P. Rinsland, M. A. H. Smith, D. C. Benner, V. M. Devi, J. M. Flaud, C. Camy-Peyret, A. Perrin, A. Goldman, S. T. Massie, L. R. Brown, and R. A. Toth, "The HITRAN molecular database: editions of 1991 and 1992," J. Quant. Spectrosc. Radiat. Transfer **48,** 469–507 (1992).
10. G. R. Janik, C. B. Carlisle, and T. F. Gallagher, "Two-tone frequency modulation spectroscopy," J. Opt. Soc. Am. B **3,** 1070–1074 (1986).
11. D. E. Cooper and R. E. Warren, "Frequency modulation spectroscopy with lead-salt diode lasers: a comparison of single tone and two-tone techniques," Appl. Opt. **26,** 3726–3732 (1987).
12. D. E. Cooper and R. E. Warren, "Two-tone optical heterodyne spectroscopy with diode lasers: theory of line shapes and experimental results," J. Opt. Soc. Am. B **4,** 470–480 (1987).
13. V. Dana, J.-Y. Mandin, C. Camy-Peyret, J.-M. Flaud, J. P. Chevillard, R. L. Hawkins, and J.-L. Delfau, "Measurements of collisional linewidths in the ν_2 band of H_2O from Fourier-transformed flame spectra," Appl. Opt. **31,** 1928–1936 (1992).
14. A. S. Pine, "Self-, N_2, O_2, H_2, and He broadening in the ν_3 band Q branch of CH_4," J. Chem. Phys. **97,** 773–785 (1992).
15. D. C. Benner, C. P. Rinsland, V. M. Devi, M. A. H. Smith, and D. Atkins, "A multispectrum nonlinear least squares fitting technique," J. Quant. Spectrosc. Radiat. Transfer **53,** 705–721 (1995).
16. M. Carlotti, "Global-fit approach to the analysis of limb-scanning atmospheric measurements," Appl. Opt. **27,** 3250–3254 (1988).
17. X. Ouyang and P. L. Varghese, "Reliable and efficient program for fitting Galatry and Voigt profiles to spectral data on multiple lines," Appl. Opt. **28,** 1538–1545 (1989).
18. D. S. Baer and R. K. Hanson, "Tunable diode laser absorption diagnostics for atmospheric pressure plasmas," J. Quant. Spectrosc. Radiat. Transfer **47,** 455–475 (1992).
19. M. P. Arroyo and R. K. Hanson, "Absorption measurements of water-vapor concentration, temperature, and line-shape parameters using tunable InGaAsP diode laser," Appl. Opt. **32,** 6104–6116 (1993).
20. R. H. Dicke, "The effect of collisions upon the Doppler width of spectral lines," Phys. Rev. **89,** 472–473 (1953).
21. K. J. Ritter and T. D. Wilkerson, "High-resolution spectroscopy of the oxygen A band," J. Mol. Spectrosc. **121,** 1–19 (1987).
22. T. Giesen, R. Schieder, G. Winnewisser, and K. M. T. Yamada, "Precise measurements of pressure broadening and shift for several H_2O lines in the ν_2 band by argon, nitrogen, oxygen, and air," J. Mol. Spectrosc. **153,** 406–418 (1992).
23. V. G. Avetisov, A. I. Nadezhdinskii, A. N. Khusnutdinov, P. M. Omarova, and M. V. Zyrianov, "Diode laser spectroscopy of water vapor in 1.8 μm: line profile measurements," J. Mol. Spectrosc. **160,** 326–334 (1993).
24. A. S. Pine, V. N. Markov, G. Buffa, and O. Tarrini, "N_2, O_2, H_2, Ar, and He broadening in the ν_1 band of NH_3," J. Quant. Spectrosc. Radiat. Transfer **50,** 337–348 (1993).
25. E. I. Moses and C. L. Tang, "High sensitivity laser wavelength modulation spectroscopy," Opt. Lett. **1,** 115–117 (1977).
26. G. C. Bjorklund, "Frequency-modulation spectroscopy: a new method for measuring weak absorptions and dispersions," Opt. Lett. **5,** 15–17 (1980).
27. G. R. Janik, C. B. Carlisle, and T. F. Gallagher, "Two-tone frequency modulation spectroscopy," J. Opt. Soc. Am. B **3,** 1070–1074 (1986).
28. D. E. Cooper and J. P. Watjen, "Two-tone optical heterodyne spectroscopy with a tunable lead-salt diode laser," Opt. Lett. **11,** 606–608 (1986).
29. L. Wang, H. Riris, C. B. Carlisle, and T. F. Gallagher, "Comparison of approaches to modulation spectroscopy with GaAlAs semiconductor lasers: application to water vapor," Appl. Opt. **27,** 2071–2077 (1988).
30. J. A. Silver, "Frequency modulation spectroscopy for trace species detection: theory and comparison among experimental methods," Appl. Opt. **31,** 707–717 (1992).
31. D. S. Bomse, A. C. Stanton, and J. A. Silver, "Frequency modulation and wavelength modulation spectroscopies: comparison of experimental methods using a lead salt diode laser," Appl. Opt. **31,** 718–731 (1992).
32. F. S. Pavone and M. Inguscio, "Frequency and wavelength modulation spectroscopies: comparison of experimental methods using an AlGaAs diode laser," Appl. Phys. B **56,** 118–122 (1993).
33. M. Gehrtz, G. C. Bjorklund, and E. A. Whittaker, "Quantum-limited laser frequency-modulation spectroscopy," J. Opt. Soc. Am. B **2,** 1510–1526 (1985).
34. P. Werle, F. Slemr, M. Gehrtz, and C. Brauchle, "Quantum-limited FM-spectroscopy with a lead-salt diode laser," Appl. Phys. B **33,** 99–108 (1989).
35. C. B. Carlisle and D. E. Cooper, "Tunable-diode-laser frequency-modulation spectroscopy using balanced homodyne detection," Opt. Lett. **14,** 1306–1308 (1989).
36. C. B. Carlisle, D. E. Cooper, and H. Preier, "Quantum noise-limited FM spectroscopy with a lead-salt diode laser," Appl. Opt. **28,** 2567–2576 (1989).
37. J. M. Supplee, E. A. Whittaker, and W. Lenth, "Theoretical description of frequency modulation and wavelength modulation spectroscopy," Appl. Opt. **33,** 6294–6302 (1994).
38. J. Reid and D. Labrie, "Second-harmonic detection with tunable diode lasers: comparison of experiment and theory," Appl. Phys. B **26,** 203–210 (1981).
39. N. Goldstein, S. Adler-Golden, J. Lee, and F. Bien, "Measurement of molecular concentrations and line parameters using line-locked second harmonic spectroscopy with an AlGaAs diode laser," Appl. Opt. **31,** 3409–3415 (1992).
40. S. Adler-Golden, J. Lee, and N. Goldstein, "Diode laser measurements of temperature dependent line parameters for wa-

ter vapor near 820 nm," J. Quant. Spectrosc. Radiat. Transfer **48,** 527–535 (1992).
41. L. C. Philippe and R. K. Hanson, "Laser diode wavelength-modulation spectroscopy for simultaneous measurement of temperature, pressure, and velocity in shock-heated oxygen flows," Appl. Opt. **32,** 6090–6103 (1993).
42. N. C. Wong and J. L. Hall, "High-resolution measurement of water-vapor overtone absorption in the visible by frequency-modulation spectroscopy," J. Opt. Soc. Am. B **6,** 2300–2308 (1989).
43. P. Kauranen and V. G. Avetisov, "Determination of absorption line parameters using two-tone frequency-modulation spectroscopy with diode lasers," Opt. Commun. **106,** 213–217 (1994).
44. V. G. Avetisov and P. Kauranen, "High-resolution measurements using two-tone frequency-modulation spectroscopy with diode lasers," submitted to Appl. Opt.
45. M.-S. Lin, S.-Y. J. Wang, and N. K. Dutta, "Measurements and modeling of the harmonic distortion in InGaAsP distributed feedback lasers," IEEE J. Quantum Electron. **26,** 998–1004 (1990).
46. G. Morthier, F. Libbrecht, K. David, P. Vankwikelberge, and R. G. Baets, "Theoretical investigation of the second-order harmonic distortion in the AM response of 1.55 μm F-P and DFB lasers," IEEE J. Quantum Electron. **27,** 1990–2002 (1991).
47. K. Y. Lau and A. Yariv, "Intermodulation distortion in a directly modulated semiconductor injection laser," Appl. Phys. Lett. **45,** 1034–1036 (1984).
48. P. L. Varghese and R. K. Hanson, "Collisional narrowing effects on spectral line shapes measured at high resolution," Appl. Opt. **23,** 2376–2385 (1984).
49. L. Galatry, "Simultaneous effect of Doppler and foreign gas broadening on spectral shapes," Phys. Rev. **122,** 1218–1223 (1961).
50. S. G. Rautian and I. I. Sobelman, "Effect of collisions on the Doppler broadening of spectral lines," Sov. Phys. Usp. **9,** 701–716 (1967).
51. F. Herbert, "Spectrum line profiles: a generalized Voigt function including collisional narrowing," J. Quant. Spectrosc. Radiat. Transfer **14,** 943–951 (1974).
52. M. Abramowitz and I. A. Stegun, eds., *Handbook of Mathematical Functions* (Dover, New York, 1972).
53. W. H. Press, B. P. Flannery, S. A. Teukolsky, and W. T. Vetterling, *Numerical Recipes* (Cambridge U. Press, Cambridge, U.K., 1989).
54. J. Humlicek, "Optimized computation of the Voigt and complex probability functions," J. Quant. Spectrosc. Radiat. Transfer **27,** 437–444 (1982); F. Schreier, "The Voigt and complex error function: a comparison of computational methods," J. Quant. Spectrosc. Radiat. Transfer **48,** 743–762 (1992).
55. E. E. Whiting, "An empirical approximation to the Voigt profile," J. Quant. Spectrosc. Radiat. Transfer **8,** 1379–1384 (1968); J. J. Olivero and R. L. Longbothum, "Empirical fits to the Voigt line width: a brief review," J. Quant. Spectrosc. Radiat. Transfer **17,** 233–236 (1977).
56. J. H. Shaw, N. Tu, and D. L. Agresta, "Sources of systematic errors in line intensities," Appl. Opt. **24,** 2437–2441 (1985).
57. C. L. Brummel and L. A. Philips, "Error analysis in rotationally resolved spectra: least-squares and Monte Carlo methods," J. Mol. Spectrosc. **159,** 287–299 (1993).
58. M. Osinski and J. Buus, "Linewidth broadening factor in semiconductor lasers: an overview," IEEE J. Quantum Electron. **QE-23,** 9–29 (1987).
59. W. Lenth, "High frequency heterodyne spectroscopy with current-modulated diode lasers," IEEE J. Quantum Electron. **QE-20,** 1045–1050 (1984).
60. S. Kobayashi, Y. Yamamoto, M. Ito, and T. Kimura, "Direct frequency modulation in GaAlAs semiconductor lasers," IEEE J. Quantum Electron. **QE-18,** 582–595 (1982).
61. M. Imai and K. Kawakita, "Measurement of direct frequency modulation characteristics of laser diodes by Michelson interferometry," Appl. Opt. **29,** 348–353 (1990).